NASA TR R-139

NATIONAL AERONAUTICS AND SPACE ADMINISTRATION

TECHNICAL REPORT
R-139

THE THEORY OF INDUCED LIFT AND MINIMUM INDUCED DRAG OF NONPLANAR LIFTING SYSTEMS

By CLARENCE D. CONE, JR.

1962

For sale by the Superintendent of Documents, U.S. Government Printing Office, Washington 25, D.C. Yearly subscription, $15; foreign, $19; single copy price varies according to size - - - - - - - - - Price 40 cents

ERRATA

NASA Technical Report R-139

THE THEORY OF INDUCED LIFT AND MINIMUM INDUCED DRAG OF NONPLANAR LIFTING SYSTEMS

By Clarence D. Cone, Jr.
1962

Page 7, column 1, equation (24): The term $\frac{\Gamma}{d\xi}$ before the bracket should be corrected as follows:

$$\frac{d\Gamma}{d\xi}$$

NASA-Langley, 1963

Issued 8-16-63

TECHNICAL REPORT R-139

THE THEORY OF INDUCED LIFT AND MINIMUM INDUCED DRAG OF NONPLANAR LIFTING SYSTEMS

By CLARENCE D. CONE, JR.

Langley Research Center
Langley Station, Hampton, Va.

CONTENTS

TECHNICAL REPORT R-139

THE THEORY OF INDUCED LIFT AND MINIMUM INDUCED DRAG OF NONPLANAR LIFTING SYSTEMS

By CLARENCE D. CONE, Jr.

SUMMARY /6288

The basic theory of the induced lift and drag of nonplanar, circulation lifting systems is developed, and methods are evolved for determining the span force loading intensity necessary for minimum induced drag. It is shown that the aerodynamic efficiency of such optimally loaded systems can be expressed in terms of an effective aspect ratio which depends in value upon the spatial distribution of the vorticity of the system. Methods for determining the maximum effective aspect ratio of arbitrary lifting systems of given span by use of conformal transformation and electrical potential-flow analog techniques are developed and illustrated. The value of the induced-drag efficiency factor is determined for the families of circular, semiellipse, and complete-ellipse arcs and for several more complex forms. The results of the theory are interpreted in terms of the physical airfoil requirements necessary for successful realization of the theoretical induced-drag reductions.

The practical application aspects of nonplanar wing systems are briefly considered.

INTRODUCTION

The requirements of many modern aircraft missions are such that high values of aerodynamic efficiency must be obtained with aircraft having wings of relatively restricted span lengths. In many of these missions the aircraft must operate at relatively large values of the lift coefficient, and the large induced drag associated with the small span consequently results in a rather low value for the operational aerodynamic efficiency. In endeavoring to increase the flight efficiency of such aircraft, it becomes necessary to investigate more complex and unconventional wing forms which might offer the possibility of securing appreciable reductions in the induced drag, subject to the restriction of limited span length. Such forms are to be found among the various nonplanar lifting systems in which the lifting surfaces have an appreciable curvature or extension in a vertical plane perpendicular to the direction of flight.

This paper has as its primary objective, therefore, the development of the quantitative theoretical procedures by which the minimum induced drag of arbitrary nonplanar lifting systems can be determined (subject to the physical restraint imposed by limiting the allowable projected span of the system). With these procedures, the optimum spatial distribution of vorticity, corresponding to the minimum induced drag for a given lift, can be obtained for any system. Both conformal transformation and electrical analog techniques are developed for determining the optimum vorticity intensities of the system, and their use is illustrated by calculating the induced-drag efficiency factor for several complex, nonplanar wing systems. In order that the theoretical treatment be reasonably self-contained and in order that the effects of spanwise curvature on the induced flow field may be made clear, the general theory of induced forces on nonplanar wings is developed in some detail for the case of a lifting arc, and the general lift and induced-drag integrals are derived for the case of wings possessing an arbitrary circulation distribution.

The theoretical developments in this paper are based upon the assumption of inviscid, incompressible fluid flow so that the results are directly applicable to subsonic flight in air. The general nature of the results, however, makes them

equally applicable to the design of water-based lifting systems such as hydrofoil planes and other submerged lifting systems. Linear vortex theory, assuming small induced velocities compared with the free-stream velocity, is used throughout.

This report is intended purely as a generalized development of the procedures by which the minimum induced drag of nonplanar wing systems can be determined. It is not the intention here to make any detailed investigation of the relative induced-drag efficiencies of particular nonplanar wings. By way of illustration of the procedures, however, the induced-drag efficiency factor is determined for a few arbitrarily selected systems. The general methods derived herein can be applied as desired to the investigation and evaluation of specific lifting systems intended for particular aircraft applications.

As an indication of the various factors affecting the physical design of actual nonplanar wing systems, a brief consideration of the practical application aspects of such wings is also presented.

SYMBOLS

A	aspect ratio
A'	curved-span aspect ratio, b'^2/S
A_{eff}	effective aspect ratio
a	circle radius in conformal transformations
B	a constant, $\int_{-1}^{1} \frac{\Gamma}{\Gamma_o} d\gamma$
b	wing span of flat wing
b'	projected wing span of nonplanar wing
C_D	drag coefficient
C_{Dp}	aircraft parasite-drag coefficient
C_{Do}	wing profile-drag coefficient
C_L	wing lift coefficient
C_1, C_2	constants
D	drag force
D_i, $\mathbf{D}_i$	induced-drag force (boldface symbol denotes vector)
D'_i, $\mathbf{D}'_i$	induced-drag force loading intensity (boldface symbol denotes vector)
d	camber depth
E	modulus of elasticity; also electric potential
e	eccentricity of an ellipse
F', $\mathbf{F}'$	aerodynamic force loading intensity (boldface symbol denotes vector)
$\mathbf{F}'_n$	aerodynamic force intensity component normal to $\mathbf{V}$ (see eq. (4))
$\mathbf{F}'_p$	aerodynamic force intensity component parallel to $\mathbf{V}$ (see eq. (5))
g	gap distance in biplanes
h	a constant, $\frac{l}{a}$
I	area moment of inertia
$i=\sqrt{-1}$	
K	a constant, BN_A
K_e	a constant (see eq. (97))
k	span efficiency factor
L, $\mathbf{L}$	lift force (boldface symbol denotes vector)
L', $\mathbf{L}'$	lift-force loading intensity (boldface symbol denotes vector)
L_i	induced lift force
L'_o	lift loading intensity in plane of symmetry
l	distance in the Joukowski transformation
M	bending moment
N_A	a constant (see eq. (42))
$\mathbf{n}$	a normal unit vector
P, P'	points in space
p	a constant (eq. (58))
q, $\mathbf{q}$	total velocity (boldface symbol denotes vector)
$\mathbf{q}_s$	bound-vortex induced velocity vector
$\mathbf{q}_\Sigma$	vortex-sheet induced velocity vector
r, $\mathbf{r}$	distance in induced-velocity equation (boldface symbol denotes vector)
S	wing area
$\mathbf{S}$	vector of surface area
s, s'	arc-length coordinates
s_t, s'_t	arc-length coordinates of wing tip
s_T	total arc span length
$\mathbf{t}$	unit tangent vector of arc
V, $\mathbf{V}$	free-stream velocity (boldface symbol denotes vector)
v_T	tangential velocity of vortex flow
W	complex potential function of a flow
w_o, $\mathbf{w}_o$	free-stream vertical flow velocity about wakes (boldface symbol denotes vector)
y, z	Cartesian coordinates
z'	complex variable, $y+iz$
β	camber factor
Γ	circulation distribution function
Γ_{max}	maximum value of circulation
Γ_o	value of circulation in plane of symmetry

γ	nondimensional Cartesian coordinate, $2y/b'$
Δ	denotes an increment
δ	nondimensional Cartesian coordinate, $2z/b'$
ϵ	electric intensity vector
ζ	vorticity vector
ζ	complex variable, $\eta+i\xi$
ζ_o	complex coordinate of center of circle in conformal transformations
ξ, η	Cartesian coordinates of ζ-plane
θ	angle of inclination of $\mathbf{r}$ (fig. 4)
λ	nondimensional Cartesian coordinate, $2\eta/b'$
ρ	mass density of fluid
σ	nondimensional Cartesian coordinate, $2\xi/b'$
τ	arc slope angle, $\tan^{-1}(dz/dy)$
φ	velocity potential
Ω_Σ	vorticity intensity vector of vortex sheet
ψ	span ratio factor, b/b'
ω	angle between tangent and secant vector of arc (fig. 36)
∇	the del operator

Superscript:

P	denotes point at which velocity is specified

Subscripts:

e	electrical analog quantity
eff	effective value
i	induced quantity
max	maximum
P, P'	denotes conditions at a specific point in space
w	wing property
1, 2, 3, 4	denotes end point of path of integration
∞	denotes condition at infinity
o	denotes value of quantity in plane of symmetry

FUNDAMENTAL THEORETICAL CONSIDERATIONS

In this section, theoretical relations are derived for calculating the lift and induced-drag relationship for nonplanar lifting systems which possess a known distribution of circulation. The general case of determining the lift and induced drag of systems with an arbitrary circulation distribution is considered first. Then the more specific case of determining the circulation distribution for minimum induced drag is investigated by use of Munk's induced-drag theorems.

Before entering into the theoretical development, however, a discussion of the basic problem of increasing the overall efficiency of actual wing systems is presented so that the physical significance of the subsequent theoretical predictions of induced drag can be properly interpreted.

THE EFFICIENCY LIMITS OF PHYSICAL WING SYSTEMS

The requirements for obtaining high aerodynamic efficiency with a conventional flat-span wing can be seen from the expression for the wing drag polar

$$C_{D,w}=C_{Do}+\frac{C_L^2}{\pi kA}$$

where C_{Do}, the profile-drag coefficient, is a function of C_L. Obviously, it is desirable for C_{Do} to be as small as possible and the effective aspect ratio kA to be as large as possible. These two requirements are incompatible, however. The thickness ratio of a wing increases as the aspect ratio is increased, and since the value of C_{Do} increases with thickness ratio, a point is ultimately reached where increases in geometric aspect ratio (or span length) are actually detrimental since the increase in profile drag becomes larger than the induced-drag reduction. In addition, for a constant wing area the structural weight of the wing must increase as the aspect ratio increases and this requirement necessitates operation at a higher value of C_L for a given flight dynamic pressure and payload weight, with a consequent increase in induced drag. When all these structural-aerodynamic interactions are taken into account in the design of an aircraft intended to fulfill a specific set of mission requirements, the analysis results in the determination of an optimum wing form with specified span b, wing area S, and aspect ratio A. The overall aircraft range and endurance parameters then become

$$\frac{L}{D}=\frac{C_L}{C_{Dp}+C_{Do}+\frac{C_L^2}{\pi kA}}$$

$$\frac{L^{3/2}}{D}=\frac{C_L^{3/2}}{C_{Dp}+C_{Do}+\frac{C_L^2}{\pi kA}}$$

If the value of C_{Dp} is considered to be independent of the lifting system for a given aircraft, improvements in aerodynamic efficiency can come

only from use of more efficient wings. With the assumption then that an optimum flat wing has been selected for a given aircraft mission, the question arises as to whether other wing forms exist which would possess less drag for the same operating conditions of cruise flight. In order to have a higher efficiency at cruise than the optimum flat wing, a lifting system must offer a significant decrease in at least one of the factors C_{D_0} or $\frac{C_L^2}{\pi kA}$ without simultaneously increasing the other to such an extent that the beneficial effect is cancelled. The coefficient $\frac{C_L^2}{\pi kA}$ implicitly involves not only the effective aspect ratio kA of the system, but also the wing structural weight which in turn helps to determine the value of C_L for cruise. Increased structural weights, of course, mean larger values of C_L for cruise, with an attendant induced-drag increase.

The following theoretical considerations show that there exist an infinite number of lifting systems which possess less *induced* drag for a given lift than the optimum flat wing (elliptical planform) of *equal span*. In fact, many nonplanar wing forms exist which are more efficient, from the induced-drag standpoint, than optimum flat wings with greater spans. However, such nonplanar wing forms must also be considered in terms of their structural weights and profile-drag coefficients in any practical, overall efficiency comparison with a flat-span wing. Clearly, the possibility of realizing net efficiency gains with nonplanar wings depends critically upon the ability to construct such forms with sufficiently low structural weights and physical surface areas, as compared with flat wings. Since the nature of the necessary design compromises of wing area and structural weight is determined by the specific mission requirements for a particular aircraft, no general statement can be made a priori about the net efficiency gains which can be anticipated with nonplanar systems. The value of nonplanar wing forms for particular applications depends upon the nature of the specific mission involved and each application must therefore be considered as a separate case.

The subsequent theoretical predictions are indicative only of the induced-drag efficiencies of nonplanar systems and must, therefore, be interpreted in light of the preceding discussion when such forms are considered for specific applications. The induced-drag efficiency factors of the sequel, however, are developed in a form which is particularly suitable for such overall design analysis.

THE INDUCED VELOCITY

Consider first an arbitrary length of a bound-vortex arc (representing a cambered-span airfoil) having a prescribed circulation distribution $\Gamma(s)$ and situated in a plane perpendicular to a steady free-stream flow of velocity $\mathbf{V}$. Since the vortex filaments composing the arc cannot terminate in the flow, there must emanate from the arc a vortex sheet whose intensity in the immediate vicinity of the arc is given by $d\Gamma/ds$ taken along the arc (fig. 1). According to the law of induced velocity, the entire flow field is specified by

$$\mathbf{q}=\mathbf{V}+\frac{1}{4\pi}\iint^{\Sigma}\boldsymbol{\Omega}_{\Sigma}\times\frac{\mathbf{r}}{r^3}\,dS+\frac{1}{4\pi}\int^{s}\Gamma(s)\,\mathbf{t}\times\frac{\mathbf{r}}{r^3}\,ds \qquad (1)$$

where $\iint^{\Sigma}$ denotes area integration over the semi-infinite vortex sheet, $\int^{s}$ denotes line integration along the bound arc, and $\mathbf{t}$ is the unit tangent vector along the arc. By the Kutta-Joukowski theorem, the bound-vortex arc will be subjected at each point of its length to an aerodynamic force whose loading intensity $\mathbf{F}'$ is

$$\mathbf{F}'(s)=\rho\mathbf{q}(s)\times\Gamma(s)\mathbf{t} \qquad (2)$$

where $\mathbf{q}(s)$ is the total velocity at points along the arc.

Since, in general, the velocity field $\mathbf{q}$ is not uniform, the wake will react upon itself to produce a continuous distortion of the vortex sheet, and this distortion will be reflected in an alteration of $\mathbf{F}'(s)$ as is evident from equations (1) and (2). The nature of such interactions is discussed in reference

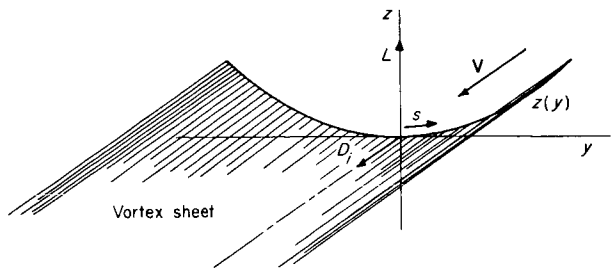

FIGURE 1.—The vortex and force system of a lifting arc.

1 for the particular case of an elliptically loaded straight vortex line.

Linearizing assumptions.—If, however, the rate of variation of the circulation along the bound arc $d\Gamma/ds$ is relatively small and the value of $\mathbf{V}$ relatively large, then the value of $\mathbf{q}_\Sigma(s)$, the wake induced velocity at the arc, as given by

$$\mathbf{q}_\Sigma(s)=\frac{1}{4\pi}\iint^{\Sigma}\boldsymbol{\Omega}_\Sigma\times\frac{\mathbf{r}}{r^3}\,dS \tag{3}$$

will be small compared with $\mathbf{V}$. The rate of deformation and inclination of the wake will then be sufficiently small that such deformation effects can be neglected and the vortex sheet assumed to extend unaltered to infinity, parallel to $\mathbf{V}$ in the downstream direction. Also, if the arc is relatively flat, the self-induction effects of the bound arc vorticity will be negligible; that is, $\mathbf{q}_s \ll \mathbf{V}$. When such conditions are fulfilled, the vortex velocity-force system can be "linearized" and the aerodynamic force intensity components $\mathbf{F}'_n$ and $\mathbf{F}'_p$ (normal and parallel, respectively, to the free-stream velocity $\mathbf{V}$) then become

$$\mathbf{F}'_n=\rho\mathbf{V}\times\Gamma\mathbf{t} \tag{4}$$

$$\mathbf{F}'_p=\rho\mathbf{q}_\Sigma\times\Gamma\mathbf{t} \tag{5}$$

For the particular case of a flat lifting-line segment, equations (4) and (5) reduce to the familiar forms

$$\mathbf{L}'=\rho\mathbf{V}\times\Gamma\mathbf{t} \tag{6}$$

$$\mathbf{D}'_i=\rho\mathbf{q}_\Sigma\times\Gamma\mathbf{t} \tag{7}$$

for the lift and induced-drag loading intensities.

Under linearizing assumptions, the aerodynamic force component acting on the bound arc in the direction normal to the free-stream velocity $\mathbf{V}$ is given by

$$\mathbf{L}=\int^{s}[(\rho\mathbf{V}\times\Gamma\mathbf{t})\cdot\mathbf{n}]\mathbf{n}\,ds \tag{8}$$

where $\mathbf{n}$ is a unit vector which specifies the direction chosen to define the lift force $\mathbf{L}$. The component acting parallel to $\mathbf{V}$ is given by

$$\mathbf{D}_i=\int^{s}[\rho\mathbf{q}_\Sigma\times\Gamma\mathbf{t}]\,ds \tag{9}$$

where $\mathbf{D}_i$ is by definition the induced drag.

Physical wing systems.—In most practical applications of lifting systems, the maximum attainable value of Γ is sufficiently small that use of the linear relations is quite valid. Linear theory, assuming small induced velocities compared with $\mathbf{V}$ and negligible wake deformations, will therefore be used in the remainder of this paper.

In the theoretical treatment of lifting systems, the physical wings are replaced by a system of bound vortices which is assumed to be rigidly fixed in a steady flow and hence capable of sustaining an aerodynamic load. For cases where the spans of the various lifting surfaces comprising the physical system are large relative to the maximum operational value of the circulation Γ_{max}, the physical wings may be replaced by individual vortex lines possessing equivalent circulation distributions. For more detailed analyses, or when the circulation is large compared with the span (highly loaded spans), the chordwise or streamwise distribution of the bound vorticity must also be considered, as well as the wake deformation effects, and the system must be represented by bound-vortex surfaces. In the sequel, the systems to be discussed are limited to bound-vortex lines and arcs, and the results, therefore, apply directly to physical systems with moderate to large spans or with relatively small maximum lift coefficients. Discussion is restricted to systems possessing a plane of symmetry, and this plane is assumed to lie parallel to $\mathbf{V}$. The aerodynamic lift is then defined as the force component in this plane, acting normal to $\mathbf{V}$.

THE LIFT AND DRAG FORCES

The induced lift of nonplanar systems.—For the general nonplanar lifting system, there exist components of induced velocity $\mathbf{q}_s$ parallel to $\mathbf{V}$ due to the bound vorticity of the system itself. The source of these components is indicated in figure 2

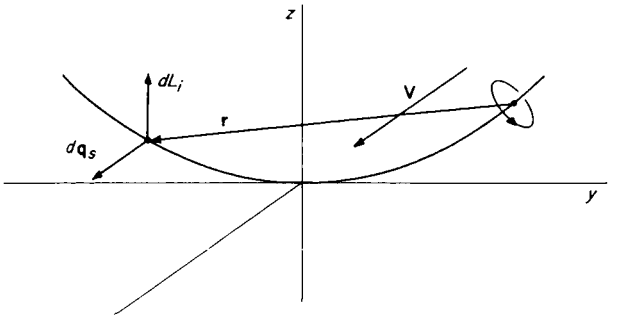

FIGURE 2.—The induced-lift velocity diagram.

for the case of an arbitrary arc shape. Under the assumptions of small induced velocities, $\mathbf{q}_s$ may usually be neglected in comparison with $\mathbf{V}$. The induced lift is considered in more detail in a subsequent section.

The induced drag of nonplanar systems.—The induced drag of nonplanar systems can be calculated, in theory, by the same methods used for planar systems, only the mathematical manipulations may become extremely complex because of the curved paths along which the integrations must be carried out. The expression for the induced drag of a symmetrical, arbitrary arc specified by $z(y)$ (fig. 3) and possessing an arbitrary circulation distribution specified by $\Gamma(s)$ is now derived to illustrate the basic effects introduced by the span curvature and to provide the fundamental integrals needed for determining the induced drag of arbitrarily loaded systems.

Consider first the differential of velocity $d\mathbf{q}_\Sigma{}^P$ (fig. 4) induced at the point $P(y,z)$ of the arc by the vortex filament of strength $\frac{d\Gamma}{ds}\,ds$ emanating from point $P'(\xi,\eta)$. The magnitude and direction of this velocity is

$$d\mathbf{q}_\Sigma{}^P=\frac{1}{4\pi}\frac{1}{r}\left(\frac{\mathbf{r}}{r}\times\frac{\mathbf{V}}{V}\right)\frac{d\Gamma}{ds}\,ds \tag{10}$$

Only a component of this velocity will be effective

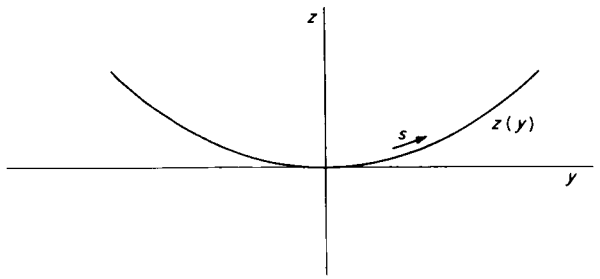

FIGURE 3.—A lifting arc of arbitrary curvature.

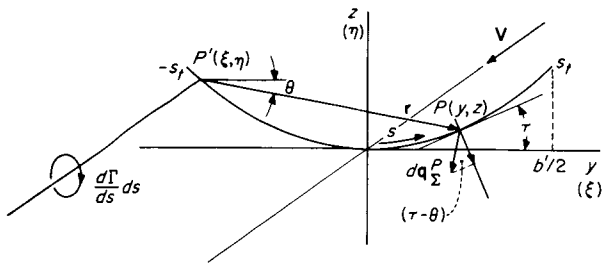

FIGURE 4.—The force and velocity relations for an arbitrary lifting arc.

in producing induced drag because of the curvature of the span. With the notation shown in figure 4 this "effective downwash" becomes, in scalar form,

$$(dq_\Sigma{}^P)_{eff}=\frac{1}{4\pi}\frac{1}{r}\cos\,(\tau-\theta)_P\frac{d\Gamma}{ds}\,ds \tag{11}$$

where the subscript P denotes conditions at the fixed point P. To obtain the total effective downwash at P due to the entire wake vorticity, equation (11) is integrated along the arc as follows:

$$(q_\Sigma{}^P)_{eff}=\frac{1}{4\pi}\int^s\frac{1}{r}\cos\,(\tau-\theta)_P\frac{d\Gamma}{ds}\,ds \tag{12}$$

Here r, θ, and $\frac{d\Gamma}{ds}$ vary with the arc coordinate s, while τ is constant for a given point P. The total induced drag is then obtained by the relation

$$D_i=\rho\int_{-s_t}^{s_t}\Gamma(s)\int_{-s_t}^{s_t}\frac{1}{4\pi}\frac{1}{r}\cos\,(\tau-\theta)_P\frac{d\Gamma}{ds'}\,ds'\,ds \tag{13}$$

where the prime denotes the variable of the inner integral and the subscript t denotes the endpoint value for the arc-length coordinate s.

In general, it is more convenient to integrate in terms of the Cartesian variables y and ξ (fig. 4). Equation (13) can therefore be transformed by use of the relations

$$ds=\sqrt{1+\left(\frac{dz}{dy}\right)^2}\,dy \tag{14}$$

$$ds'=\sqrt{1+\left(\frac{d\eta}{d\xi}\right)^2}\,d\xi \tag{15}$$

to yield

$$D_i=\frac{\rho}{4\pi}\int_{-b'/2}^{b'/2}\Gamma\sqrt{1+\left(\frac{dz}{dy}\right)^2}\int_{-b'/2}^{b'/2}\frac{1}{r}\frac{d\Gamma}{d\xi}\cos\,(\tau-\theta)_P d\xi\,dy \tag{16}$$

where

$$r=[(z-\eta)^2+(y-\xi)^2]^{1/2} \tag{17}$$

and $b'/2$ is the length of the projected span along the y (and ξ) axis. The function $\cos\,(\tau-\theta)_P$ can be expressed in terms of y, z, ξ, and η by substituting for the various terms on the right in the following identity:

$$\cos\,(\tau-\theta)_P=\cos\,\tau\cos\,\theta+\sin\,\tau\sin\,\theta \tag{18}$$

From the geometric relations of figure 4, the following relations are evident:

$$\cos \tau = \frac{1}{\left[1+\left(\frac{dz}{dy}\right)^2\right]^{1/2}} \tag{19}$$

$$\cos \theta = \frac{(y-\xi)}{[(z-\eta)^2+(y-\xi)^2]^{1/2}} \tag{20}$$

$$\sin \tau = \frac{1}{\left[1+\left(\frac{dz}{dy}\right)^{-2}\right]^{1/2}} = \frac{dz/dy}{\left[1+\left(\frac{dz}{dy}\right)^2\right]^{1/2}} \tag{21}$$

$$\sin \theta = \frac{(z-\eta)}{[(z-\eta)^2+(y-\xi)^2]^{1/2}} \tag{22}$$

Substitution of these relations into equation (18) and dropping of the subscript P, yields

$$\cos(\tau-\theta) = \frac{1}{\left[1+\left(\frac{dz}{dy}\right)^2\right]^{1/2}} \frac{(y-\xi)+\frac{dz}{dy}(z-\eta)}{[(z-\eta)^2+(y-\xi)^2]^{1/2}} \tag{23}$$

Substituting this expression into equation (16) and rearrangement gives the final relation for the induced drag in terms of the Cartesian coordinates,

$$D_i = \frac{\rho}{4\pi}\int_{-b'/2}^{b'/2}\Gamma(y)\int_{-b'/2}^{b'/2}\frac{\Gamma}{d\xi}\left[\frac{(y-\xi)+\frac{dz}{dy}(z-\eta)}{(z-\eta)^2+(y-\xi)^2}\right]d\xi\,dy \tag{24}$$

With this relation the induced drag of any airfoil whose spanwise curvature $z(y)$ is known can be calculated when the circulation loading $\Gamma(y)$ is specified. Equations (8) and (24), therefore, determine the induced-drag polar for any nonplanar wing of specified geometry.

When the fact is considered that Γ, $d\Gamma/d\xi$, z, and η may themselves be involved functions, the difficulty of obtaining an analytical solution for equation (24) is obvious and, in general, machine computation must be used. In addition, the so-called "principal value" of the inner integral must be taken and this operation requires the use of special techniques. Equation (24) applies directly only to the case of a single lifting arc. For the case of two superposed arcs, such as shown in figure 5, calculation of the total induced drag of the system requires the solution of four double integrals of the type in equation (24), two of which may be considerably more complex in form. In general, solution of a system of N superposed arcs requires the evaluation of N^2 double integrals of the type shown.

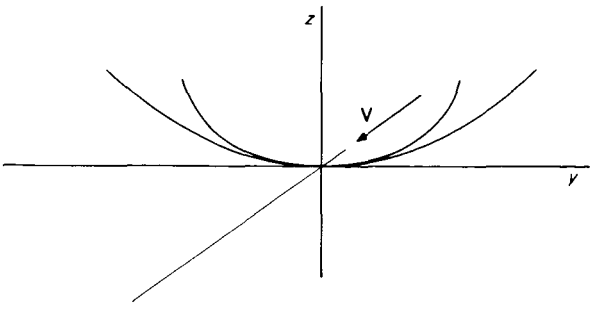

FIGURE 5.—A lifting system of superposed arcs.

In many cases of practical concern, however, one is not interested in solving equation (24) or a system of such equations by using an arbitrary circulation distribution $\Gamma(y)$, but rather by using the particular distribution which will produce the minimum induced drag for the given arc geometry $z(y)$. This is particularly true in the present case, where maximum wing efficiencies are of interest. The problem of determining this optimum circulation loading for an arbitrary system of lifting lines was originally solved by Munk (ref. 2) by use of the calculus of variations. The results of Munk lead to the specification of the optimum circulation distribution and also to a simple method for determining the induced drag of the system, provided the velocity potential for the flow about the vortex wake can be determined. This method eliminates the need for direct integration of equation (24). The total results of Munk's investigation are not considered here, but two of the more basic theorems evolved are listed for use in the sequel.

Theorem 1: The total induced drag of any three-dimensional system of lifting elements is independent of the positions of the various elements in the direction of the free-stream velocity **V** (Munk's stagger theorem). Thus, if all the lifting elements of a system are translated, parallel to **V**, into a single plane normal to **V** while the initial circulation is maintained constant, the induced drag of the resulting two-dimensional system will be exactly the same as that of the three-dimensional, longitudinally dispersed system.

Theorem 2: When all the elements of a lifting system have thus been translated to a single plane, the induced drag will be a minimum when the component of induced velocity normal to the lifting element at each point is proportional to the cosine of the angle of inclination of the lifting element at that point. In terms of the velocities previously defined, the condition for minimum induced drag thus becomes

$$\int \cos\,(\tau-\theta)_P dq_{\Sigma^P}=\frac{w_o}{2}\cos\,\tau \qquad (25)$$

where $w_o/2$ is the constant of proportionality. This relation indicates that the intensity of the wake vorticity $d\Gamma/ds$ at each point P must be such that the velocity component normal to the vortex sheet is

$$(\mathbf{q}_\Sigma)_{eff}=w_o\cos\,\tau\left(\mathbf{t}\times\frac{\mathbf{V}}{V}\right) \qquad (26)$$

The condition is illustrated in figure 6 for an arbitrary arc shape.

Since the required vortex intensity $d\Gamma/ds$ corresponds to a specific circulation distribution $\Gamma(s)$ along the lifting arcs, the potential flow generated by the wake will give the desired optimum distribution $\Gamma(s)$. The potential may be determined by conformal transformations of basic flows for many simple lifting systems. To obtain the optimum circulation distribution, a conformal transformation which will transform a known basic flow into the flow about the desired wake form is found, using the "free-stream" two-dimensional vertical flow of magnitude $-w_o$. The resulting transformed flow will then satisfy the requirement of equation (26) and will correspond to the potential flow around a solid boundary having the same shape as the wake from the lifting system.

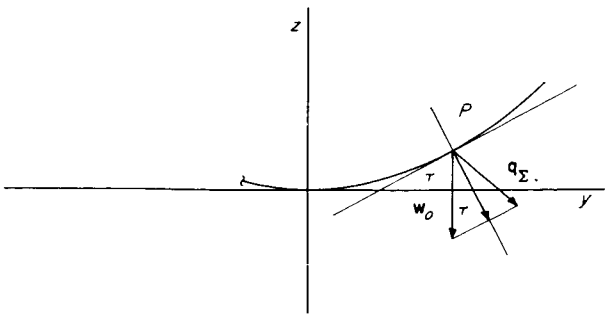

FIGURE 6.—The effective-downwash relation for minimum induced drag.

The velocity potential φ of the transformed flow can be found at once from that of the basic flow. In particular, since by definition

$$\Gamma_P=\oint\mathbf{q}\cdot d\mathbf{s}=(\varphi_2-\varphi_1)_P \qquad (27)$$

the desired distribution of Γ along all lifting lines is determined. Further development and application of these results is carried out in the following sections.

THE PRINCIPLE OF VORTICITY ATTENUATION

WAKE ENERGY AND CIRCULATION RELATIONS

Consider a flat lifting line operating with any arbitrary symmetrical distribution of circulation $\Gamma(y)$. Let the maximum value of this function be Γ_{max} (not necessarily the value for $\Gamma(0)$). The law of vortex continuity requires that all the vortex filaments comprising the line continue downstream unaltered in strength. Thus, the circulation in any circuit surrounding the vortex wake leaving a semispan (fig. 7) must be equal to the circulation existing at the center of the span $\Gamma_o=\Gamma(0)$ by Stokes' theorem,

$$\Gamma_o=\iint^S\boldsymbol{\zeta}\cdot d\mathbf{S}$$

and the total circulation of the wake vorticity cannot be altered. The kinetic-energy content of the wake, however, corresponding to the induced drag on the wing, may vary considerably even for a constant value of Γ_o, depending upon the form of the function $\Gamma(y)$. Thus, even though two wings may have equal values of lift and Γ_o, their induced-drag values may be quite different. The circulation value and the lift do not in general uniquely determine the induced drag; $\Gamma(y)$ is also very important.

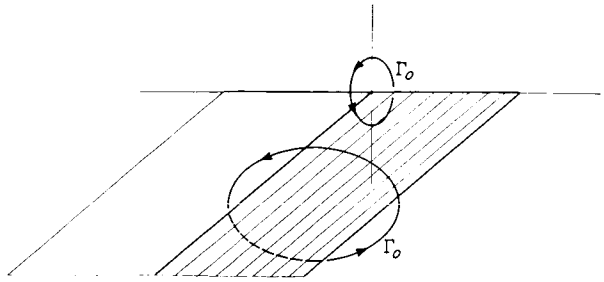

FIGURE 7.—The relation of wake and bound vorticity.

A simple illustration of this fact is the Rankine vortex flow. If the core diameter of such a vortex is specified along with the intensity of the vorticity, the circulation Γ and kinetic energy of the total flow are determined. If a second vortex of larger core diameter but of equal circulation is considered (fig. 8), it is evident that the kinetic energy of the second flow will be less even though it possesses the same circulation as the first. Thus, if these two vortices are considered as the wakes from two different wings (ref. 1), it is apparent that the induced drag of two lifting systems can be varied considerably by changes in the spatial distribution of the trailing vorticity. These facts are pointed out here merely to emphasize that despite the need to preserve the total wing circulation, no unique restriction is placed upon the induced drag which accompanies this circulation.

Effects of spreading vortex wakes.—The effective downwash producing induced drag on an element of a lifting line at point P due to a vortex line of strength $d\Gamma$ at point P' (fig. 4) is

$$(dq_{\Sigma^P})_{eff}=\left(\frac{1}{4\pi}\frac{1}{r}\frac{d\Gamma}{ds}\,ds\right)\frac{\mathbf{r}}{r}\times\frac{\mathbf{V}}{V}\cdot\mathbf{n}$$

where $\mathbf{n}$ is a unit vector normal to the lifting element at P; $\mathbf{n}=\mathbf{t}\times\frac{\mathbf{V}}{V}$. In order to minimize $(dq_{\Sigma^P})_{eff}$ and hence the induced-drag differential, three conditions are desirable: (1) the value of $d\Gamma/ds$ should be small, (2) the length r should be large, and (3) the vectors $\frac{\mathbf{r}}{r}$ and $\mathbf{n}$ should be as nearly parallel as possible. These conditions can be satisfied by spreading the lifting elements over as large an area as possible.

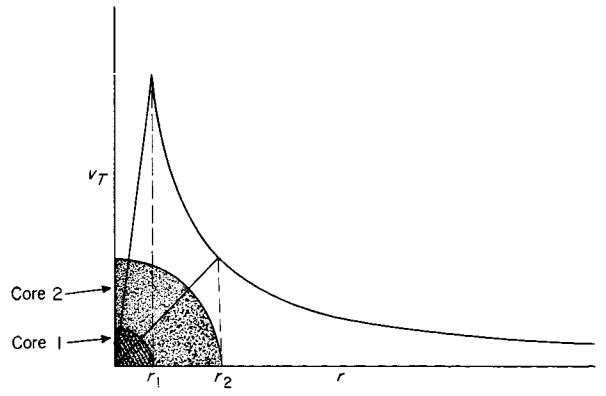

FIGURE 8.—The velocity distribution for two vortices of different radius.

An example of the practical application of this principle is the biplane wing. If, for illustration, an elliptically loaded vortex line possessing a maximum circulation Γ_o (fig. 9) is split into two separate elliptically loaded lines with equal maximum circulations of $\frac{1}{2}\Gamma_o$ and separated vertically by a distance g, then for any pair of interacting vortex elements v_1 and v_2 it is seen that the above three requirements are fulfilled. The intensity of each trailing vortex filament has been reduced, the distance r has been increased, and the vectors $\frac{\mathbf{r}}{r}$ and $\mathbf{n}$ are more nearly parallel. As the distance g is increased, or as the number of separate lifting lines is increased (multiplanes), the efficiency of the system of course increases. A second practical example is the wing with an end plate (fig. 10). The same principle of diffusing or spreading the vortex lines of the wake is used to reduce the induced drag of the wing. The vortex filaments of the main lifting line branch at the end plate as shown, so that for a given value of Γ_o, $\frac{d\Gamma}{ds}$ along the main span is less than for the plane wing.

Wake momentum—kinetic-energy relation.—The principle just asserted is in reality merely a

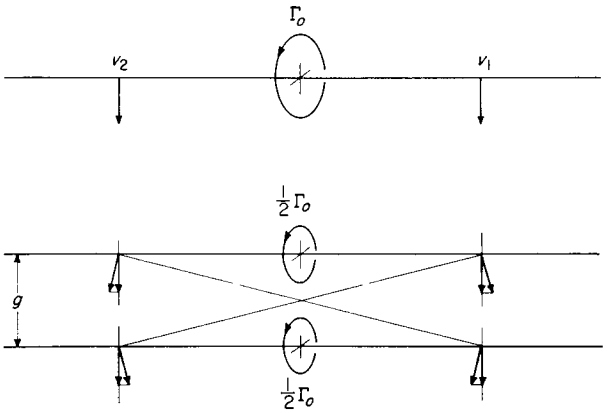

FIGURE 9.—Attenuation of vorticity by a biplane wing.

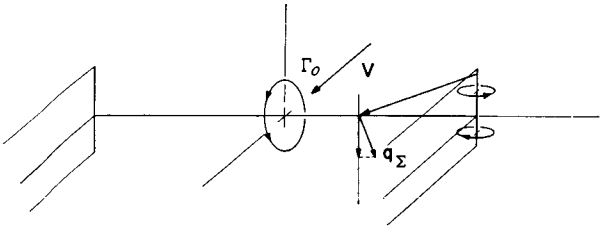

FIGURE 10.—Attenuation of vorticity by use of end plates.

direct consequence of the momentum—kinetic-energy relation for airfoil wakes (ref. 2, appendix B). In order to produce a given lift force an airfoil must impart a definite vertical momentum increase to the airstream, and the kinetic energy of the wake motion must come from the thrust work done by the wing in overcoming the induced drag. For a given momentum change, the wake kinetic energy will decrease if the wake vertical velocity is decreased while the mass of air affected is increased. In vorticity spreading, such as caused by increasing the span of a wing with constant lift, the local induced wake velocities are reduced since the intensity of the vorticity at any point is lowered (fig. 8), and a larger mass of air is affected. Thus, the total kinetic-energy content of a unit length of the wake is decreased by vorticity spreading while the lift is unaffected.

In the development of various lifting-system configurations which will possess increased aerodynamic efficiency, therefore, only those which satisfy the principle of vorticity spreading or attenuation may be expected to have decreased induced drag. A generalized treatment of the relation between airfoil drag and wake energy is given in reference 3.

THE EFFECTIVE ASPECT RATIO OF NONPLANAR LIFTING SYSTEMS

THE LIMITING CASE OF THE ELLIPTICALLY LOADED LINE

By application of theorem 2 of the preceding discussion it can be proved that the optimum circulation distribution for a flat lifting line is elliptical in form:

$$\Gamma(y)=\Gamma_o\sqrt{1-\left(\frac{2y}{b}\right)^2} \tag{28}$$

Since both τ and θ are zero for a flat line, equation (25) reduces to the requirement that

$$q_z{}^P=\frac{w_o}{2} \tag{29}$$

so that the downwash must be constant across the span. When the potential of the flow about a flat plate wake is determined, the elliptical distribution of equation (28) results. Since the downwash is constant across the span, it follows that the desired Γ distribution is obtained by use of the elliptical-planform wing and that the elliptical lift-loading-intensity distribution

$$L'(y)=L'_o\sqrt{1-\left(\frac{2y}{b}\right)^2} \tag{30}$$

will give the minimum induced drag for flat or planar monoplane wings.

It is shown in three-dimensional airfoil theory (ref. 4) that the lift and induced drag of an elliptically loaded flat wing are

$$L=\frac{\pi}{4}\rho V\Gamma_o b \tag{31}$$

$$D_i=\frac{\pi}{8}\rho\Gamma_o{}^2 \tag{32}$$

where b is the span length. Since the wing aspect ratio is defined by

$$A=\frac{b^2}{S} \tag{33}$$

where S is the wing area, the corresponding lift and drag coefficients become

$$C_L=\frac{\pi}{2}\frac{\Gamma_o}{bV}A \tag{34}$$

$$C_{Di}=\frac{\pi}{4}\frac{\Gamma_o{}^2}{b^2V^2}A \tag{35}$$

The resulting induced-drag polar is therefore given by

$$C_{Di}=\frac{C_L{}^2}{\pi A} \tag{36}$$

This expression is actually a special case of a more general relation which will be derived subsequently, and serves as a convenient basis for comparing the efficiencies of various lifting systems.

OPTIMALLY LOADED NONPLANAR SYSTEMS

The drag polar.—In order to determine the induced-drag polar corresponding to the optimum circulation loading for a nonplanar wing, such as represented by the generalized arc of figure 11, use is made of the basic relation of theorem 2

$$\frac{F'}{D'_i}=\frac{2V}{w_o\cos\tau} \tag{37}$$

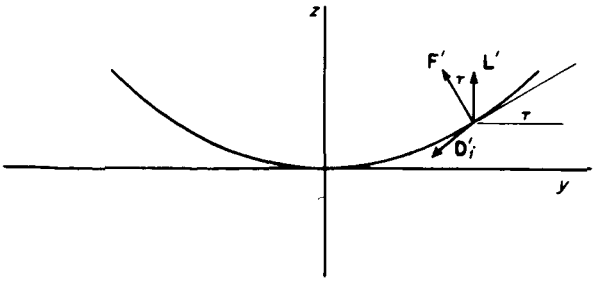

FIGURE 11.—The relation between the aerodynamic force and the lift.

where F' is the aerodynamic force loading intensity. Since $F' \cos \tau = L'$, this relation may be rewritten as

$$\frac{D_i'}{L'} = \frac{w_o}{2V} \tag{38}$$

where $w_o/2V$ is a constant. Therefore the ratio D_i'/L' is constant at each point of the arc, and thus the total induced drag can be written as

$$D_i = L \frac{w_o}{2V} \tag{39}$$

Equation (39) can be expanded to give

$$D_i = \frac{L^2}{2\rho \dfrac{V^2}{w_o} \displaystyle\int_{-b'/2}^{b'/2} \Gamma(y)dy} \tag{40}$$

where the factor 2 corrects for the velocity w_o which applies to the doubly infinite vortex wake of a two-dimensional flow, as will be clear from the illustrations of the next sections. This drag relation can be nondimensionalized by using the relation $\gamma = \dfrac{y}{b'/2}$, to yield

$$D_i = \frac{L^2}{2\rho V^2 \dfrac{\left(\dfrac{\Gamma_o}{w_o}\right)}{\left(\dfrac{b'}{2}\right)} \left(\dfrac{b'}{2}\right)^2 \displaystyle\int_{-1}^{1} \frac{\Gamma}{\Gamma_o} d\gamma} \tag{41}$$

Let

$$\frac{\Gamma_o/w_o}{b'/2} = N_A \tag{42}$$

and

$$\int_{-1}^{1} \frac{\Gamma}{\Gamma_o} d\gamma = B \tag{43}$$

then

$$D_i = \frac{L^2}{\frac{1}{2}\rho V^2 (b')^2} (BN_A)^{-1} \tag{44}$$

The induced-drag polar can therefore be written as

$$C_{Di} = \frac{C_L^2}{KA'} \tag{45}$$

where $K = BN_A$ and $A' = \dfrac{b'^2}{S}$. The factor A' may be called the geometric aspect ratio of the curved span.

The effective aspect ratio.—Comparison of equation (45) with equation (36) suggests the concept of the effective aspect ratio A_{eff} for evaluating the efficiency of nonplanar lifting systems. If the same wing area S and span b of an elliptical planform flat wing of aspect ratio A are also used as the basis for calculating the coefficients of a nonplanar system of span b' (as indicated in fig. 12), the following relations can be defined

$$b = \psi b' \tag{46}$$

$$A' = \frac{1}{\psi^2} \frac{b^2}{S} = \frac{A}{\psi^2} \tag{47}$$

Equation (45) then becomes

$$C_{Di} = \frac{C_L^2}{\dfrac{K}{\psi^2} A} \tag{48}$$

Thus, the induced-drag polar for any nonplanar system can be expressed as

$$C_{Di} = \frac{C_L^2}{\pi k A} \tag{49}$$

where A is the aspect ratio of the given flat, elliptically loaded wing being used for comparison, and

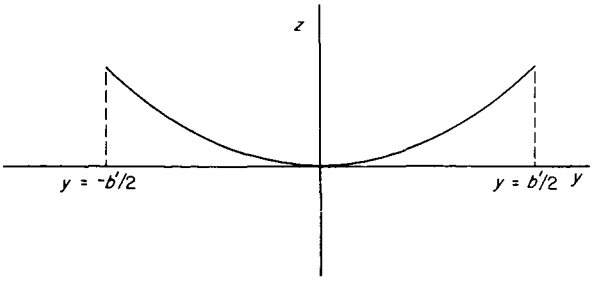

FIGURE 12.—The span of a nonplanar wing.

k is an efficiency factor which is constant as long as the optimum circulation distribution exists on the nonplanar lifting system, where

$$k=\frac{1}{\psi^2\pi}\frac{\left(\frac{\Gamma_o}{w_o}\right)}{\left(\frac{b'}{2}\right)}\int_{-1}^{1}\frac{\Gamma}{\Gamma_o}\,d\gamma \tag{50}$$

Since the coefficients C_L and C_{Di} for the flat and nonplanar wings are based on the same area, the two systems being compared will experience equal lifts at equal values of C_L and dynamic pressure. But for cases where $k>1$, the nonplanar system will be more efficient than the optimum flat wing; that is, the nonplanar system will have less induced drag than the flat elliptical wing for equal total lift forces. If $k<1$, the nonplanar system will be less efficient. These facts may be simply expressed in terms of the effective aspect ratio A_{eff}, where

$$A_{eff}=kA \tag{51}$$

so that

$$C_{Di}=\frac{C_L^2}{\pi A_{eff}} \tag{52}$$

It is obvious from the preceding development that any nonplanar lifting system of span b' can be compared with any flat-span elliptical wing of span b and area S. However, the usual problem which is of primary interest is that, given a particular flat-span elliptical wing (the most efficient flat wing), how do various modifications affect the efficiency of the wing, and in particular, what modifications will result in an increase in efficiency. Since certain modifications may result in a span change, such as curving a flat wing into an arc while keeping the total arc length equal to the length of the original flat span, the factor ψ is necessary to account for span-change effects. When comparing systems in which the spans are held equal, $\psi=1.0$. The particular convenience of the definition of k, as given by equation (50), for comparison purposes will be evident in the subsequent theoretical development.

In these derivations, no mention has been made of the physical nature of the nonplanar lifting system. Indeed, the induced drag of the system is dependent only on the spatial intensity distribution of the lift (or aerodynamic force) and is quite independent of the physical means used to produce this distribution. Transformation of a given spatial distribution of circulation into a physical lifting system can be accomplished in, theoretically, an infinite number of ways, but, in the usual case practical considerations and compromises determine the manner in which this must be done. The preceding theory, however, provides all the basic information needed for design purposes. Practical application aspects are considered in the last section of this paper. The problem of determining the circulation distribution necessary for obtaining the maximum effective aspect ratio of an arbitrary system is now considered.

DETERMINATION OF THE SPAN LOADING DISTRIBUTION FOR MINIMUM INDUCED DRAG

The conditions of theorem 2 for minimum induced drag require that the vorticity distribution in the wake be such that $\mathbf{q}_\Sigma\cdot\mathbf{n}=w_o\cos\tau$ at every point of the wake. Thus, far downstream of the lifting system the wake will move normal to itself locally with a velocity $w_o\cos\tau$.

It is assumed here, of course, that the wake inclination and deformation effects are negligible. Then the effective induced flow at the lifting system will be $(w_o\cos\tau)/2$, since the vortex wake is only semi-infinite with respect to the plane containing the system (all longitudinally distributed lifting elements having been translated into a single plane, by theorem 1).

If a plane is taken far downstream normal to the wake, the flow will consist of the two-dimensional motion due to the wake vortex lines. The section of the wake made by this plane will be exactly the same as that of the lifting system (fig. 13). If a vertical flow $-\mathbf{w}_o$ is now superposed on this two-dimensional wake flow, the

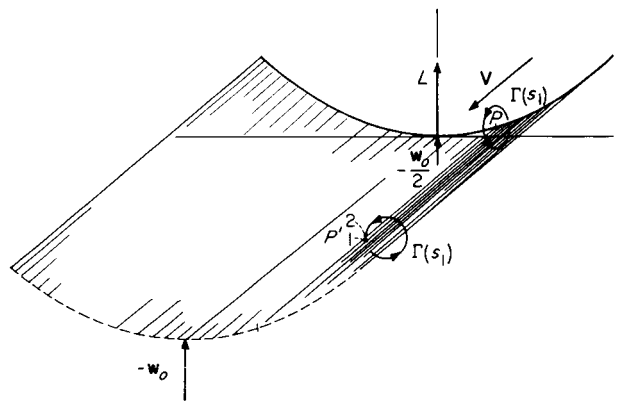

FIGURE 13.—The flow regime for calculation of the potential distribution along a lifting arc.

wake will be brought to rest so that the flow will be steady, and the resulting velocity field will correspond to the potential flow about a solid boundary having the same section shape as does the wake. Thus the jump in potential φ at any point of the wake (fig. 13), or at any point of the analogous solid boundary, specifies the circulation at the corresponding point in the bound-vortex system since

$$\Gamma_P=(\varphi_2-\varphi_1)_{P'} \tag{53}$$

The vertical flow in the plane of the lifting system will be $-\mathbf{w}_o/2$, or half that existing far downstream. Determination of the potential of the two-dimensional wake flow therefore establishes the value of k corresponding to minimum induced drag, according to equation (50).

Determination of the velocity potential φ for arbitrary flows is in general difficult, but can be carried out for many simple lifting line systems by conformal mapping. To establish the potential, a transformation must be found which will carry a basic, known flow with "free-stream" velocity $-\mathbf{w}_o$ into the desired flow in the transformed plane while preserving the flow $-\mathbf{w}_o$ at infinity. Then at corresponding points in the two flows the same velocity potential and stream function values apply so that Γ becomes known for the lifting system (transformed plane) by means of equation (53). Use of conformal mapping for determining the optimum Γ loadings and corresponding k values for lifting arcs and closed lifting lines is illustrated in the next section.

In general, the transformation function necessary to obtain the flow about arbitrary forms cannot be found easily. This situation is especially true for complex systems such as superposed lifting arcs and lines. There exists, however, a quite satisfactory solution to this problem. By use of the electrical potential-flow analog, the potential distribution for even complex systems can be determined easily. With this device, advantage is taken of the fact that the flow of electrical current in a uniformly conducting medium is directly analogous to incompressible fluid flow since both satisfy Laplace's equation $\nabla^2\varphi=0$. When identical boundary conditions are imposed on the two flows, measurements of the electrical potential along the boundary can be converted directly to the velocity potential distribution along the boundary (lifting system) in the analogous fluid flow. The principle of this method and its application to the solution of a number of complex systems is illustrated in the next section.

659943—63——3

SOLUTIONS FOR THE EFFECTIVE ASPECT RATIO OF OPTIMALLY LOADED ARCS

The first class of nonplanar lifting systems that will be investigated by means of the foregoing theory consists of symmetrical arc segments. Such forms are of particular interest because of the simplicity of construction of the airfoils which may be derived from them and because the mechanical design of such wings follows closely the usual procedures for flat wings. In addition, the effects of such factors as dihedral angle and aeroelastic deformation of the span on conventional flat airfoil efficiency can be estimated with simple arc forms. As special cases of arc forms, the efficiency factor for lifting lines which form closed ellipses will be investigated for the family $0\leqq e\leqq 1$ where e is the eccentricity. The circle will be included as a lower limit ($e=0$) and the straight line as the upper limit ($e=1$) of the ellipse forms.

SOLUTIONS BY CONFORMAL TRANSFORMATION

In order to illustrate the application of conformal mapping techniques to the solution of equation (50), the k values of the family of circular arcs and the family of closed ellipses will be determined.

Circular-arc segments.—For present purposes, the family of lifting lines represented by circular-arc segments can be expressed in terms of a camber factor β, where as shown in figure 14

$$\beta=\frac{d}{b'/2} \tag{54}$$

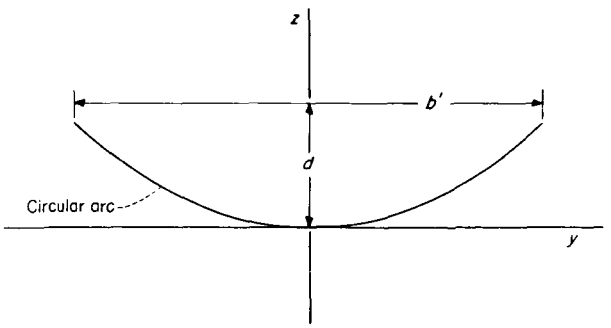

FIGURE 14.—Distances used to define the camber factor of a circular-arc segment.

The ratio of depth d to projected semispan length $b'/2$, therefore, defines each specific arc of the family as the arcs proceed from a straight line ($\beta=0$) to a semicircle ($\beta=1$) for the range

$$0\leqq\beta\leqq 1 \tag{55}$$

In order to determine the potential distribution along any member of this family of arcs, the two-dimensional flow about a circle in the ζ-plane (fig. 15) is transformed into the flow around the desired arc in the z'-plane by means of the Joukowski transformation

$$z'=\zeta+\frac{l^2}{\zeta} \tag{56}$$

Here $\zeta(=\xi+i\eta)$ and $z'(=y+iz)$ are complex variables. The Joukowski transformation will transform the circle of radius a whose center is located on the positive η-axis and which passes through the point l on the ξ-axis (i.e., the point $\xi=l$) into a circular-arc segment in the z'-plane, as shown in figure 15. In particular, the point $\zeta=l$ will transform into the point $z'=2l=\frac{b'}{2}$. Thus the camber factor can be written as

$$\beta=\frac{d}{b'/2}=\frac{2\sqrt{a^2-l^2}}{2l} \tag{57}$$

since the distance d is twice the η coordinate of the circle center in the ζ-plane. The radius a becomes a function of β by the following definitions:

$$a=pl \tag{58}$$

$$\beta=\sqrt{p^2-1} \tag{59}$$

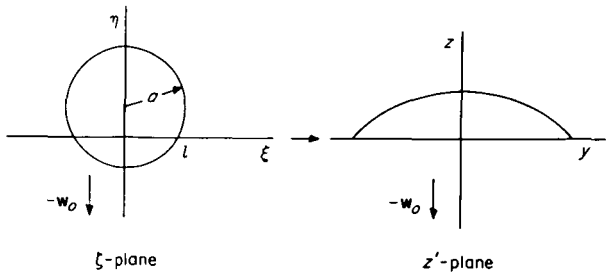

FIGURE 15.—The Joukowski transformation relations for circular-arc segments.

or

$$p=+\sqrt{1+\beta^2} \qquad (1\leqq p\leqq\sqrt{2}) \tag{60}$$

and

$$a=l\sqrt{1+\beta^2} \tag{61}$$

The circle center is located at $\zeta=\zeta_o=i(\sqrt{a^2-l^2})=i\beta l$.

The complex potential of the flow about the circle in the ζ-plane due to a uniform flow $-w_o$ from infinity as shown in figure 15 is

$$W(\zeta)=iw_o\left[(\zeta-\zeta_o)-\frac{a^2}{(\zeta-\zeta_o)}\right] \tag{62}$$

(The flow and arc in the z'-plane are inverted here, but this inversion has no effect on the determination of Γ.) The velocity potential φ is, therefore,

$$\varphi(\xi,\eta)=\mathrm{R}[W(\zeta)]=w_o\left[(\eta-\beta l)+\frac{a^2(\eta-\beta l)}{\xi^2+(\eta-\beta l)^2}\right] \tag{63}$$

where R denotes the real part of $W(\zeta)$. This equation can be nondimensionalized by dividing all terms by $b'/2$. With the definitions

$$\lambda=\frac{\eta}{b'/2} \tag{64}$$

$$\sigma=\frac{\xi}{b'/2} \tag{65}$$

and after rearrangement, equation (63) becomes

$$\frac{\varphi}{w_o\frac{b'}{2}}=\lambda-\frac{\beta}{2}+\frac{p^2}{4}\frac{\left(\lambda-\frac{\beta}{2}\right)}{\sigma^2+\left(\lambda-\frac{\beta}{2}\right)^2} \tag{66}$$

since $a^2=p^2l^2$ and $l=\frac{1}{2}\left(\frac{b'}{2}\right)$.

The equation of the circle is, in nondimensional form,

$$\lambda=\pm\left(\frac{p^2}{4}-\sigma^2\right)^{1/2}+\frac{\beta}{2} \tag{67}$$

for $-\frac{p}{2}\leqq\sigma\leqq\frac{p}{2}$. Under the transformation of equation (56), the corresponding points in the z'-plane

are given by the nondimensional coordinates

$$\gamma=\frac{y}{b'/2}=\sigma+\frac{\sigma/4}{(\sigma^2+\lambda^2)} \tag{68}$$

$$\delta=\frac{z}{b'/2}=\lambda-\frac{\lambda/4}{(\sigma^2+\lambda^2)} \tag{69}$$

Thus, at corresponding points (σ, λ) and (γ, δ), the velocity potential (eq. (66)) has the same value and the potential distribution along the length of any circular arc with specified β becomes known. From equation (53), the circulation distribution Γ/Γ_o can be determined. Figure 16 shows the nondimensional circulation distribution as determined by this procedure for four arcs of different camber, $\beta=0$, 0.4, 0.6, and 0.8.

From such plots, the efficiency factor k can be determined by equation (50). The value of the factor

$$\frac{(\Gamma_o/w_o)}{b'/2} \tag{70}$$

is given by the transformation for the point $z'=i(2\sqrt{a^2-l^2})$, and the integral

$$\int_{-1}^{1}\frac{\Gamma}{\Gamma_o}d\gamma \tag{71}$$

may be determined graphically or analytically from the potential distribution.

The only remaining unknown in equation (50) is the factor ψ. Since, by definition,

$$\psi=\frac{b}{b'} \tag{72}$$

the value of ψ depends upon the span b of the flat elliptically loaded line to which the circular-arc segment of projected span b' is being compared. The actual significance of this factor is discussed subsequently; but for the present, ψ is assigned the value 1.0. This value of ψ, of course, means that the circular arc is being compared with the flat line having an equal span and producing equal lift.

The variation of the efficiency factor k with the spanwise camber factor β has been determined for the entire family of circular-arc segments $(0\leqq\beta\leqq1)$, and is presented in figure 17 for the case $\psi=1.0$. The efficiency of the circular arc is seen to increase continuously with spanwise camber, reaching a maximum value of 1.50 when the arc becomes a semicircle $(\beta=1.0)$. For this case, the effective aspect ratio of the arc is 50 percent greater than

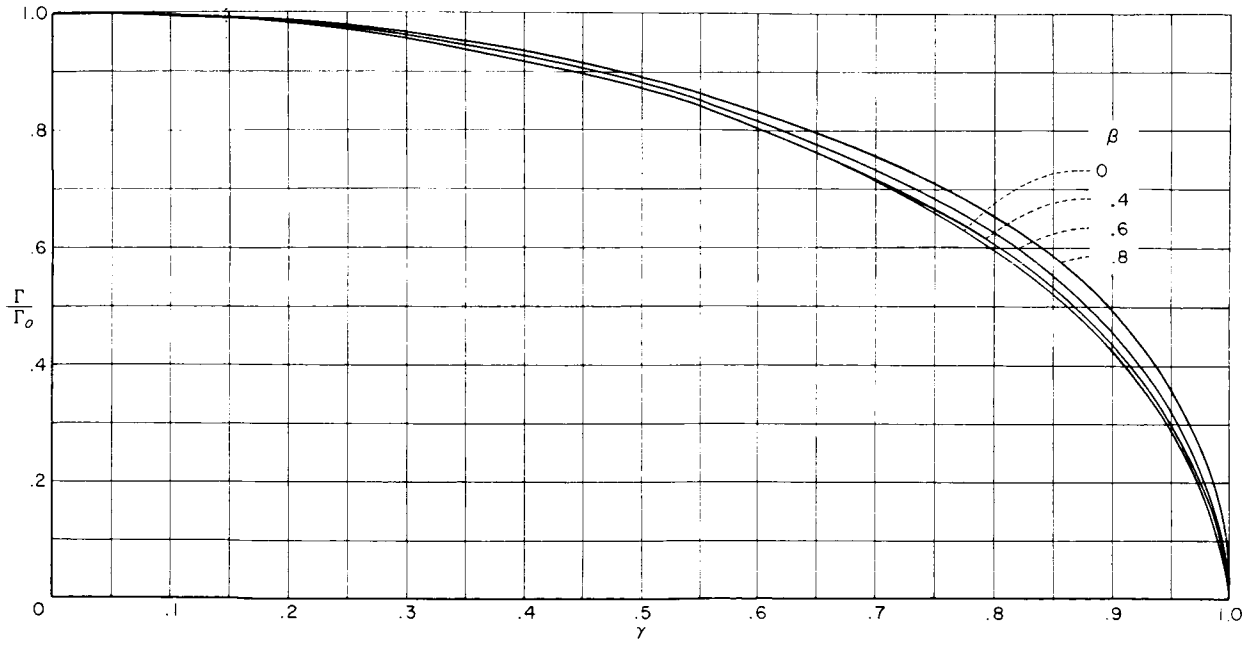

FIGURE 16.—The optimum nondimensional circulation distribution for several members of the family of circular-arc segments.

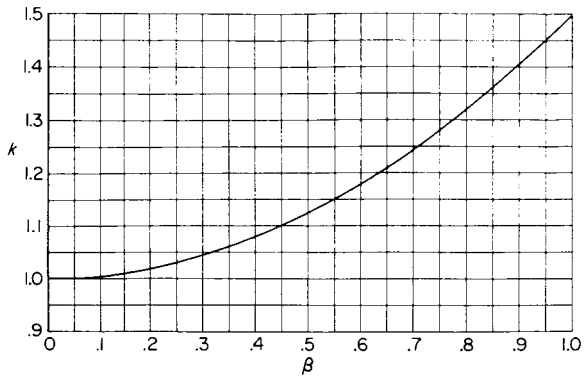

FIGURE 17.—The variation of the efficiency factor with the camber factor for the family of circular-arc segments. $\psi=1.0$.

the geometrical aspect ratio of the elliptical-planform wing of equal span ($b=b'$). Thus the optimally loaded arc having a camber factor of 1.0 will have 33.3 percent less induced drag than the flat, elliptical-planform wing producing the same total lift force. The efficiency gain for small amounts of camber is initially small, reaching a k value of only 1.05 at $\beta=0.316$. The relative curvature for various amounts of camber is indicated in figure 18.

From the results of figure 17, it appears that very sizable gains in induced-drag efficiency are aerodynamically possible with the use of circular-arc curvature of the span, provided, of course, the span is optimally loaded.

It can be shown that the curve of figure 17 is actually a branch segment of the parabola

$$k=1.00+0.50\beta^2 \tag{73}$$

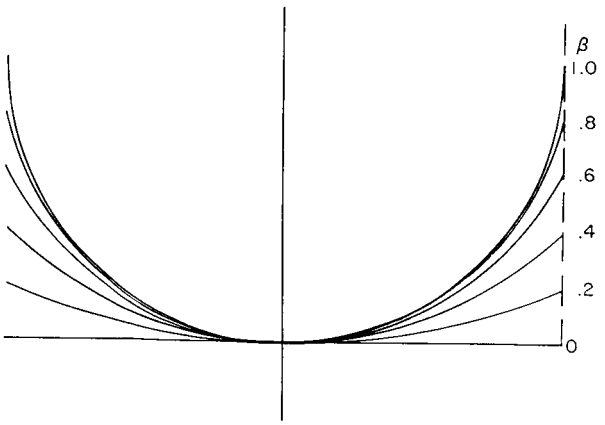

FIGURE 18.—Relative curvature of a series of circular arcs of equal span with varied camber.

for $0\leqq\beta\leqq1$, for the case where $\psi=1.0$. For other values of ψ, equation (73) becomes

$$k=\frac{(1.00+0.50\beta^2)}{\psi^2} \tag{74}$$

Complete ellipses.—A particularly interesting case of lifting arcs is obtained when the arc is extended to form a closed loop or curve. Examples are circles, ellipses, ovals, and rectangles. Such forms are capable of attaining very high values of k, much larger than those possible with arc segments of moderate curvature. On the other hand, however, the physical system needed to obtain the circulation distribution for minimum drag is much more complex.

As an extension of theorem 2, it is shown in reference 2 that the condition for minimum induced drag on a closed lifting curve is that the circulation distribution $d\Gamma/ds$ be such that the wake induced velocity is constant and equal to $\mathbf{w}_o$ (far downstream) at all points of the area enclosed by the vortex wake. Thus, the air passing through the lifting curve in the three-dimensional flow will be enclosed by the vortex sheet and will move downward with the velocity $\mathbf{w}_o$ far downstream. In the plane containing the closed lifting curve, the induced velocity at all points within the boundary area is given by

$$\mathbf{q}_z=\frac{\mathbf{w}_o}{2} \tag{75}$$

When the uniform flow $-\mathbf{w}_o$ is imposed on the wake flow, the entire wake "body" will be brought to rest and the resulting steady potential flow will yield the desired potential distribution at the lifting curve.

The Joukowski transformation (eq. (56)) will map the circle $|\zeta|=a$ into an ellipse, in the z'-plane, whose eccentricity is given by

$$e=\frac{2al}{a^2+l^2} \tag{76}$$

and whose major- and minor-axis lengths are, respectively,

$$2\frac{a^2+l^2}{a} \tag{77}$$

$$2\frac{a^2-l^2}{a} \tag{78}$$

Let $a=l/h$, where h is a constant for a given ellipse. The eccentricity then becomes, from equation (76),

$$e=2\frac{h}{(1+h^2)} \tag{79}$$

From the definition of the eccentricity, it follows that

$$\frac{1}{2}\frac{b'}{2}e=l \tag{80}$$

since the distance from the origin to a focus of the ellipse is $2l$. Thus the radius a is given as a function of h by

$$a=\frac{b'}{2}\frac{1}{(1+h^2)} \tag{81}$$

By use of the nondimensional variables

$$\lambda=\frac{\eta}{b'/2} \tag{64}$$

$$\sigma=\frac{\xi}{b'/2} \tag{65}$$

$$\frac{a}{b'/2}=\frac{1}{(1+h^2)} \tag{82}$$

the equation of the circle in the ζ-plane becomes

$$\lambda=\pm\left[\left(\frac{1}{1+h^2}\right)^2-\sigma^2\right]^{1/2} \tag{83}$$

for the range $-\left(\frac{1}{1+h^2}\right)\leqq\sigma\leqq\left(\frac{1}{1+h^2}\right)$.

The velocity potential of the ζ-plane flow is obtained from an expansion of equation (62) yielding

$$\frac{\varphi}{w_o\frac{b'}{2}}=\lambda+\frac{1}{(1+h^2)^2}\frac{\lambda}{(\sigma^2+\lambda^2)} \tag{84}$$

The points (y,z) in the z'-plane corresponding to the points (ξ,η) in the ζ-plane are given in nondimensional form by the relations

$$\gamma=\frac{y}{b'/2}=\sigma+\left(\frac{h}{1+h^2}\right)^2\frac{\sigma}{\sigma^2+\lambda^2} \tag{85}$$

$$\delta=\frac{z}{b'/2}=\lambda-\left(\frac{h}{1+h^2}\right)^2\frac{\lambda}{\sigma^2+\lambda^2} \tag{86}$$

At corresponding points (as given by eqs. (85) and (86)), therefore, the value of φ (eq. (84)) is the same and the potential distribution around the ellipse is established.

In general, it is more convenient to describe the shape of the ellipse in terms of a "camber" factor β, the same as was done for the circular arcs. Thus the camber of the ellipse is given by

$$\beta=\frac{\text{Minor axis}}{\text{Major axis}}=\sqrt{1-e^2} \tag{87}$$

The camber is an elliptical function of the eccentricity, and is plotted in figure 19. Equation (79), therefore, determines h as a function of β.

The circulation distribution $\frac{\Gamma}{\Gamma_o}(\gamma)$ is obtained by the relation

$$\frac{\Gamma}{\Gamma_o}(\gamma)=\frac{\varphi_P-\varphi_{P'}}{\varphi_{0,2}-\varphi_{0,1}} \tag{88}$$

as shown in figure 20. The value of Γ/Γ_o as a function of γ is presented in figure 21 for the range $\beta=0$ to 1.0. The case $\beta=0$ gives the elliptical distribution of the straight line. The case $\beta=1$ gives the distribution for the full circle. The intermediate cases $0<\beta<1$ apply to ellipses. It thus appears that the elliptical distribution applies to all complete ellipse forms including the special limiting cases of the line and circle. The efficiency factor k for the family of ellipses $0\leqq\beta\leqq1$ has been determined by conformal mapping and is presented in figure 22 as a function of the camber. Here again, the value of ψ has been taken as 1.0 in equation (50). The efficiency factor is obviously a linear function of the ellipse camber, and reaches a maximum value of 2.0 for the circle form ($\beta=1.0$). This value of k indicates that the lifting circle, or annular airfoil, has an effective aspect ratio 100 percent greater than the flat elliptical wing having equal span and producing equal lift. This particular result has long been known, and the possibilities of realizing such efficiency increases have prompted considerable work on ring-wing lifting systems (refs. 5 and 6, for example).

The efficiency factor for the family of ellipses can be expressed in terms of β by the relation

$$k=\beta+1 \tag{89}$$

for $0\leqq\beta\leqq1.0$, for the case where $\psi=1.0$. For

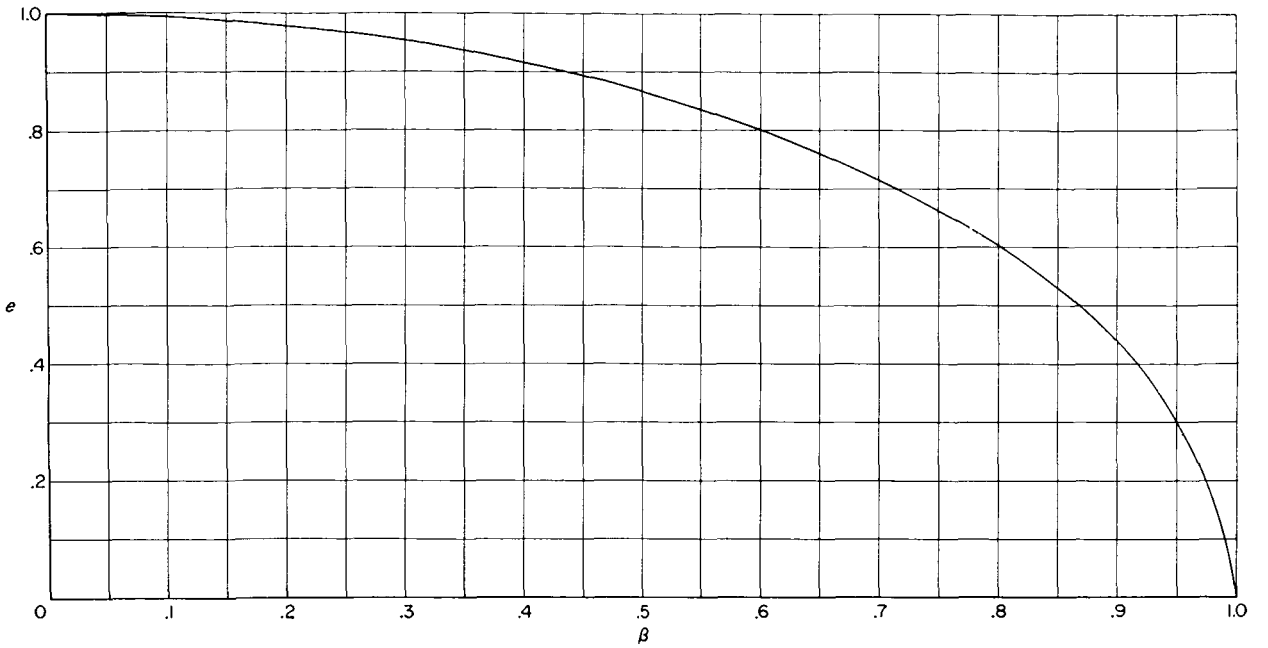

FIGURE 19.—The variation of ellipse eccentricity with the camber factor.

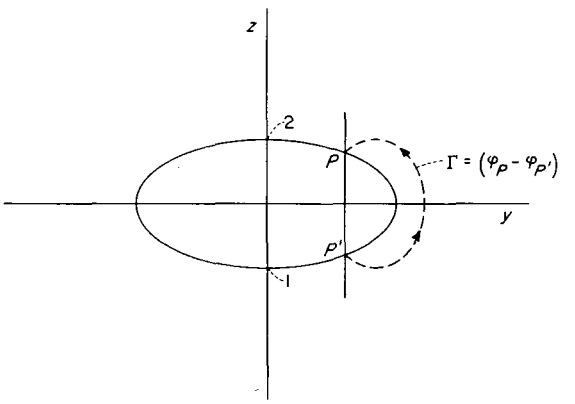

FIGURE 20.—The points used to determine the circulation loading of closed ellipses.

arbitrary values of ψ, this relation becomes

$$k=\frac{\beta+1}{\psi^2} \tag{90}$$

The considerations of this section have been limited to the calculation of the efficiency of lifting circular arcs and full ellipses by conformal transformation techniques. These forms are by no means the only ones solvable by conformal mapping, but are appropriate cases for illustrating the procedure. In general, however, it is quite difficult to determine the transformation which will give the desired z'-plane flow. A method is now discussed which allows accurate determination of the k value for any arbitrary lifting system by use of a simple electrical analogy.

SOLUTIONS BY ELECTRICAL ANALOGY

When an electrical current is passed through a uniformly conducting sheet (two-dimensional flow), it can be shown that the resulting distribution of electrical potential E must satisfy Laplace's equation

$$\nabla^2 E=0 \tag{91}$$

in two dimensions, say y and z, where the uniform flow at infinity is parallel to the z-axis. Since the velocity potential φ of two-dimensional, incompressible fluid flows also satisfies Laplace's equation

$$\nabla^2\varphi=0 \tag{92}$$

there exist the following direct analogies between the fluid and electrical flows:

Fluid Regime	Electrical Regime
$\mathbf{q}$	$\boldsymbol{\epsilon}$
$\varphi=\int^s \mathbf{q}\cdot d\mathbf{s}$	$E=\int^s \boldsymbol{\epsilon}\cdot d\mathbf{s}$
$\mathbf{q}=-\nabla\varphi$	$\boldsymbol{\epsilon}=-\nabla E$

(93)

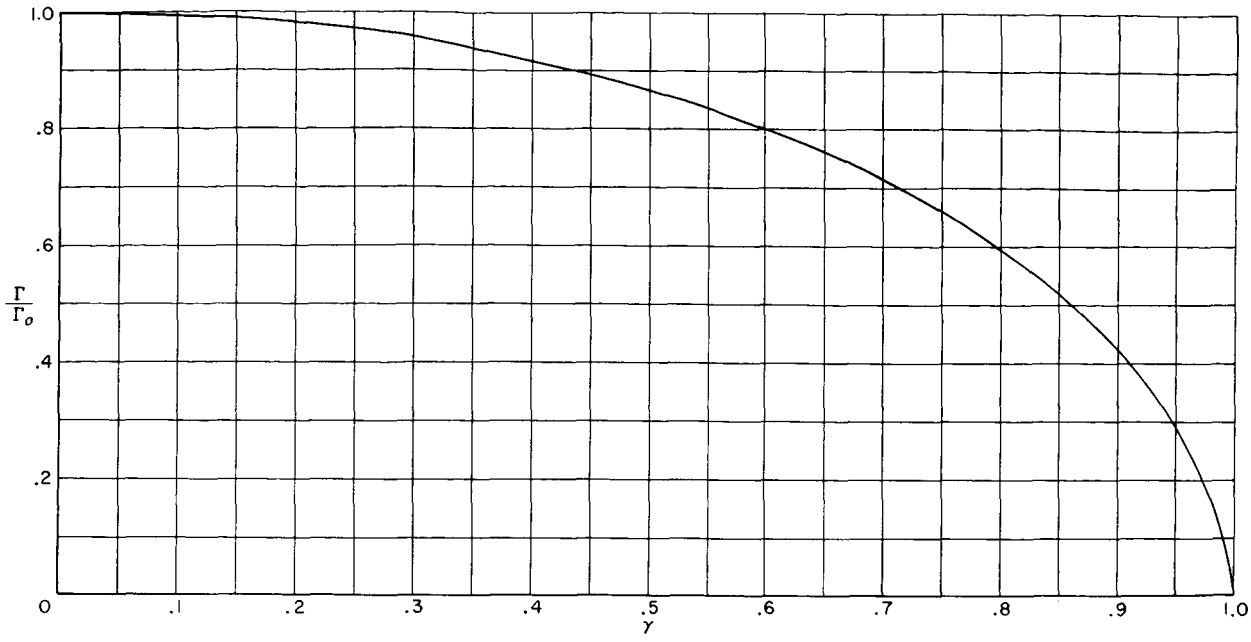

FIGURE 21.—The optimum nondimensional circulation loading for closed ellipses. $0 \leqq \beta \leqq 1.0$.

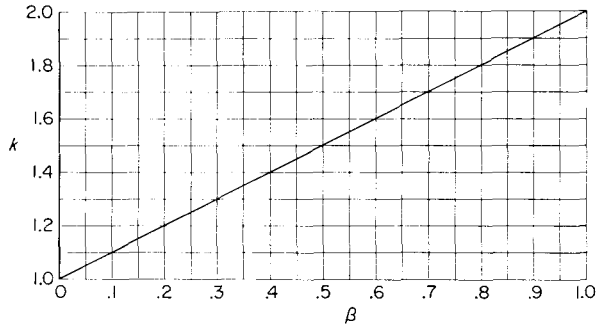

FIGURE 22.—The variation of the efficiency factor with the camber factor for the family of closed ellipses. $\psi = 1.0$.

where

ϵ electric intensity vector

E electric potential

Application of the equation of continuity to each system leads directly to equations (91) and (92)

$$\text{div } \mathbf{q} = \nabla \cdot \nabla\varphi = \nabla^2\varphi = 0 \tag{94}$$

$$\text{div } \epsilon = \nabla \cdot \nabla E = \nabla^2 E = 0 \tag{95}$$

Thus, the equipotential lines $\varphi = \text{Constant}$ in fluid flow correspond directly to the equipotential lines $E = \text{Constant}$ in electrical flow, when identical boundary conditions exist.

Analogy between aerodynamic and electric parameters.—It has been previously shown that in order to determine the value of k the dimensionless constant K has to be determined for the flow about the given boundary form (representing the lifting system), where

$$K = \frac{\left(\frac{\Gamma_o}{w_o}\right)}{\left(\frac{b'}{2}\right)} \int_{-1}^{1} \frac{\Gamma}{\Gamma_o}\, d\gamma \tag{96}$$

The electrical analog of this equation is

$$K_e = \frac{(\Delta E)_o}{\left(\frac{dE}{dz}\right)_\infty \frac{b'}{2}} \int_{-1}^{1} \frac{\Delta E}{(\Delta E)_o}\, d\gamma \tag{97}$$

where ΔE is the potential difference equivalent to Γ_P (see eq. (53)), $(\Delta E)_o$ is the potential difference across the boundary center ($\equiv \Gamma_o$), and $\left(\frac{dE}{dz}\right)_\infty$ is the change in potential per unit length in the direction of the uniform current at infinity.

Since K and K_e are both dimensionless constants, they must have the same numerical value for geometrically similar flows (equivalent boundary conditions). This fact allows the experimental determination of the value of K for any

potential flow regime. In order to construct the analogous electrical flow, a sheet of uniformly conducting material is mounted between two parallel electrodes as shown in figure 23(a). The form or boundary representing the lifting system is then cut into the conducting sheet, the size of this boundary being small compared with the dimensions of the sheet so that the flow near the outer boundaries of the sheet will be undisturbed (fig. 23(b)). The cut representing the lifting system causes the current flow to satisfy the same boundary conditions as in the fluid regime (velocity normal to the boundary is 0), and the values of ΔE, $(\Delta E)_o$, and $\left(\frac{dE}{dz}\right)_\infty$ may be read directly with a voltmeter. Thus, K_e can be evaluated by use of equation (97), and since the values of K and K_e are the same, the value of K (eq. (96)) is obtained.

The various operational details of the electrical analog system are not discussed here, as considerable information has previously been published on the practical problems attending the use of such devices for other types of potential flow studies. In general, the primary problem associated with the use of the analog is finding a perfectly uniformly conducting sheet material. There exists, however, a particularly convenient material for such applications as the present one in the form of a special conducting paper.[1] This material was used for all analog studies reported in this paper. The specific analog setup used in this investigation is pictured in figure 23(c) and was especially developed for these tests.

As an indication of the accuracy which can be achieved with the analog system pictured in figure 23(c), the distributions for $\frac{\Delta E}{(\Delta E)_o}$ as measured for the cases of a flat lifting line, a semicircle, and a full circle are presented in figure 24, where they are compared with the theoretical distributions as obtained by conformal transformations. The excellent agreement is obvious. The values of K_e as determined for these three forms are as follows:

[1] Information on this material can be obtained from the paper "Analog Field Mapping on 'Teledeltos' Recording Paper." Copies of this paper may be obtained from the Western Union Telegraph Company, Marketing Department, Government and Contract Sales, 60 Hudson St., New York 13, N.Y.

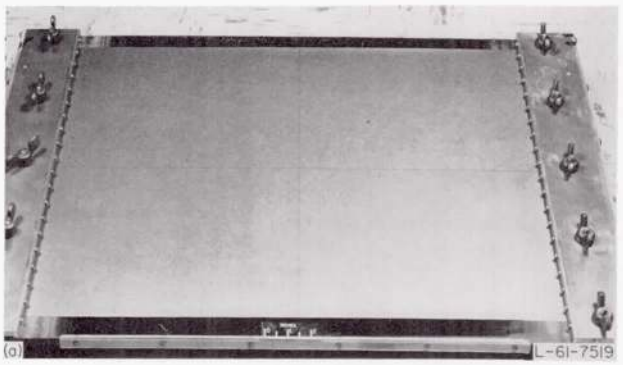

(a) The table with conducting sheet.

FIGURE 23.—The electrical analog system used to determine the optimum circulation distributions.

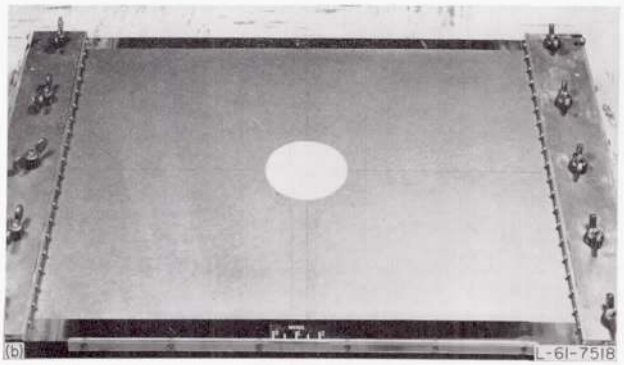

(b) The conducting sheet with a circular boundary.

FIGURE 23.—Continued.

Form	K_e (measured)	K_e (theoretical)	Percent error
Line	3. 20	3. 14	+1. 9
Semicircle	4. 83	4. 72	+2. 3
Full circle	6. 42	6. 28	+2. 2

In general, the accuracy of the values of K determined by the analog, for all forms discussed in this report, is believed to be within −1.0 percent to 3.0 percent of the true value. A positive error in K_e, or K, has the effect of making the associated value of the factor k smaller than the true value.

Semiellipse arcs.—The efficiency factor k has been determined for the family of semiellipse arcs by use of the analog method. To determine the value of K_e, a given arc (corresponding to a given value of β, the camber factor) was plotted on the conducting paper. A very narrow slit was then cut along the arc to form the electrical boundary.

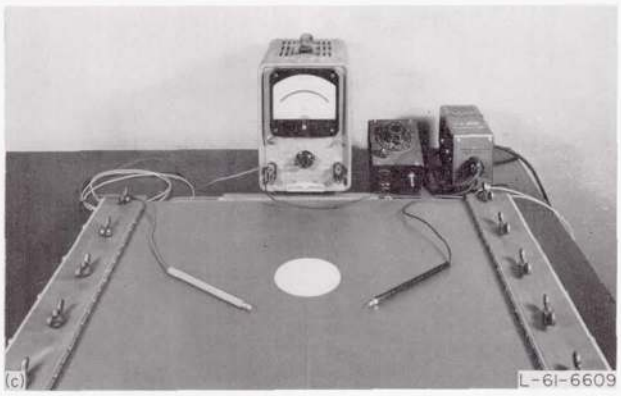

(c) The entire analog system.

FIGURE 23.—Concluded.

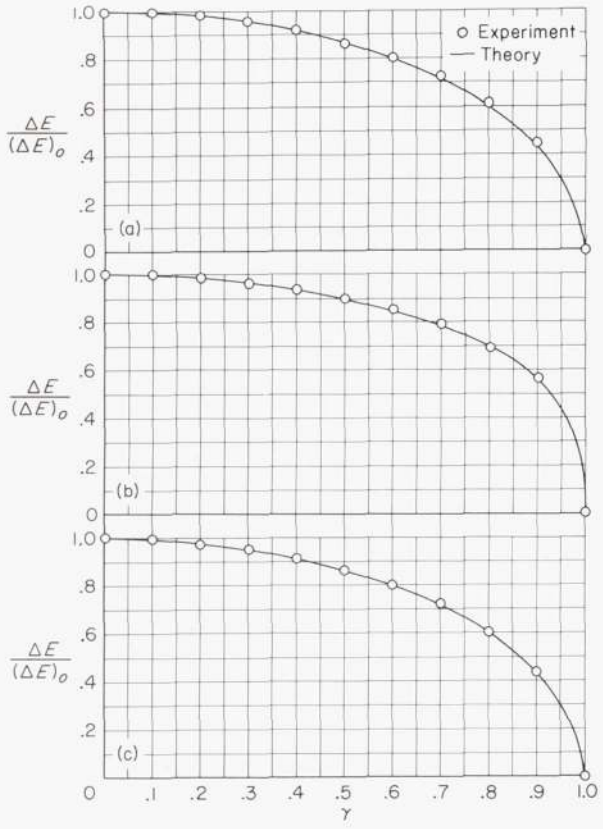

(a) Line.

(b) Semicircle.

(c) Circle.

FIGURE 24.—Comparison of the experimental analog readings with theoretical predictions.

The arcs were all constructed to the same scale with a constant semispan length of 2 inches. The potential difference was then determined for 11 equally spaced points across the semispan (including the origin) by use of finely pointed probes attached to a highly sensitive electron-tube voltmeter.

Figure 25(a) shows the plot of an arbitrary arc form from which the boundary line is cut. The slit used to represent the lifting arc line necessarily has some finite width, and while measurement of the potential difference is relatively simple for flat portions of the curves (fig. 25(b)) some question arises as to the proper position of the probes when measurements are made along the highly curved portions (fig. 25(c)). Theoretically, the measurements are to be made at a point, but physically, the measurements must be made at two separate points, one on each side of the slit. When the slit has appreciable curvature, the two points on the intersecting ordinate may become widely separated, as shown in figure 25(c). The proper position of the probes in this case is determined by the fact that the equipotential lines must be normal to the boundary in the immediate vicinity of the boundary. Thus, if at a given spanwise point where ΔE is to be read, a normal line to the curve is constructed through the point before the boundary slit is cut, the potential lines which would end on this point will lie along this normal line in the vicinity of the slit. The probes must, therefore, be placed not at points lying on the line γ=Constant, but at the intersection points of the normal line with the edges of the slit (fig. 26). The smaller the slit can be made, the less will be the error incurred by using points on the line γ=Constant, of course. All points were measured along normal lines in this investigation, even though all slits were very narrow (0.02 inch in width).

The value of K was determined by integration of the potential difference distribution

$$B_e=\int_{-1}^{1}\frac{\Delta E}{(\Delta E)_o}d\gamma \tag{98}$$

and by using the measured values of $\left(\frac{dE}{dz}\right)_\infty$, $\frac{b'}{2}$, and $(\Delta E)_o$. In practice, $\left(\frac{dE}{dz}\right)_\infty$ was taken as the voltage difference across the sheet divided by the distance (24.00 inches) between the lines of contact of the electrodes, for each individual reading.

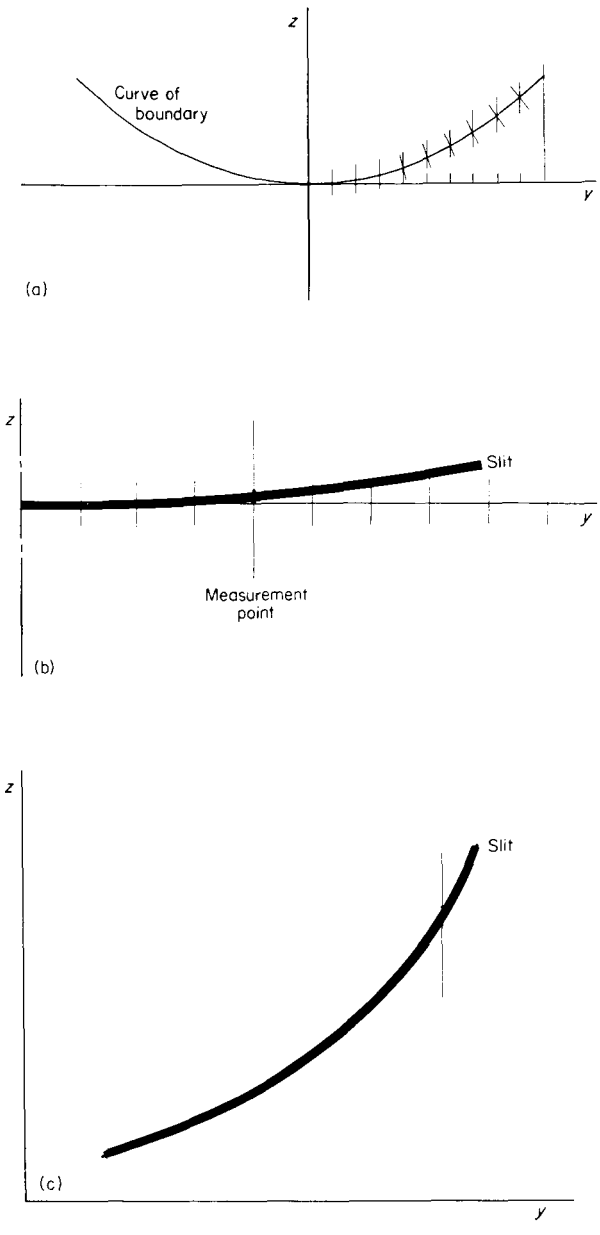

(a) Arbitrary arc form.

(b) Flat portion of slit.

(c) Highly curved portion of slit.

FIGURE 25.—The analog form preparation.

The value of k as a function of the camber β is presented in figure 27 for the family of semiellipses $0 \leqq \beta \leqq 1$, $\psi = 1.0$. The value of k reaches a maximum of 1.5 at $\beta = 1.0$, which corresponds, of course, to the previously discussed case of the semicircle. The semiellipse arcs are considerably more efficient than the circular arcs of equal span.

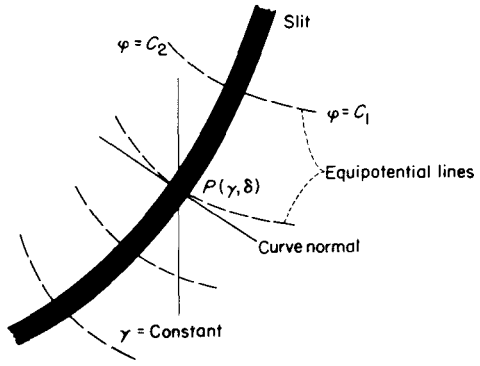

FIGURE 26.—Illustration of the method used to determine the potential distribution on analog forms.

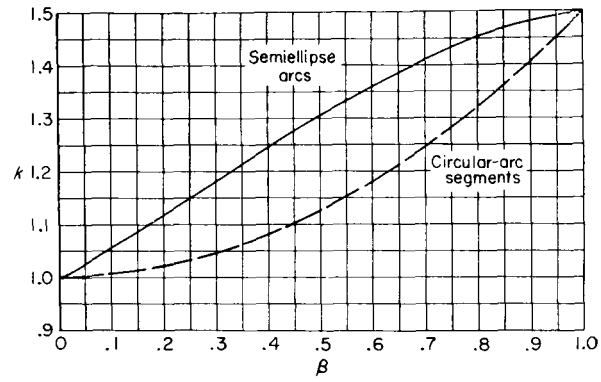

FIGURE 27.—The variation of the efficiency factor of semiellipse arcs with the camber factor. $\psi = 1.0$.

This fact is shown in figure 27 where the circular-arc efficiency is entered as a dashed curve. The superior efficiency of the semiellipse arcs may have been intuitively expected since the semiellipse arcs are less curved over the central portion where the aerodynamic force intensity is greatest; thus, more of this force acts to create lift than is the case with circular arcs. The circulation distribution $\frac{\Gamma}{\Gamma_o}(\gamma)$ is shown in figure 28 for four semiellipse arcs.

While only the specific case of semiellipses has been discussed here, obviously it is possible to treat arcs of any shape by the analog method. For example, families of arc segments of ellipses, parabolas, hyperbolas, and all other symmetrical functions can be evaluated in a simple manner. Complex lifting systems made up of a combination of such arcs can be handled in the same manner as single arcs. This subject will be discussed in the next section.

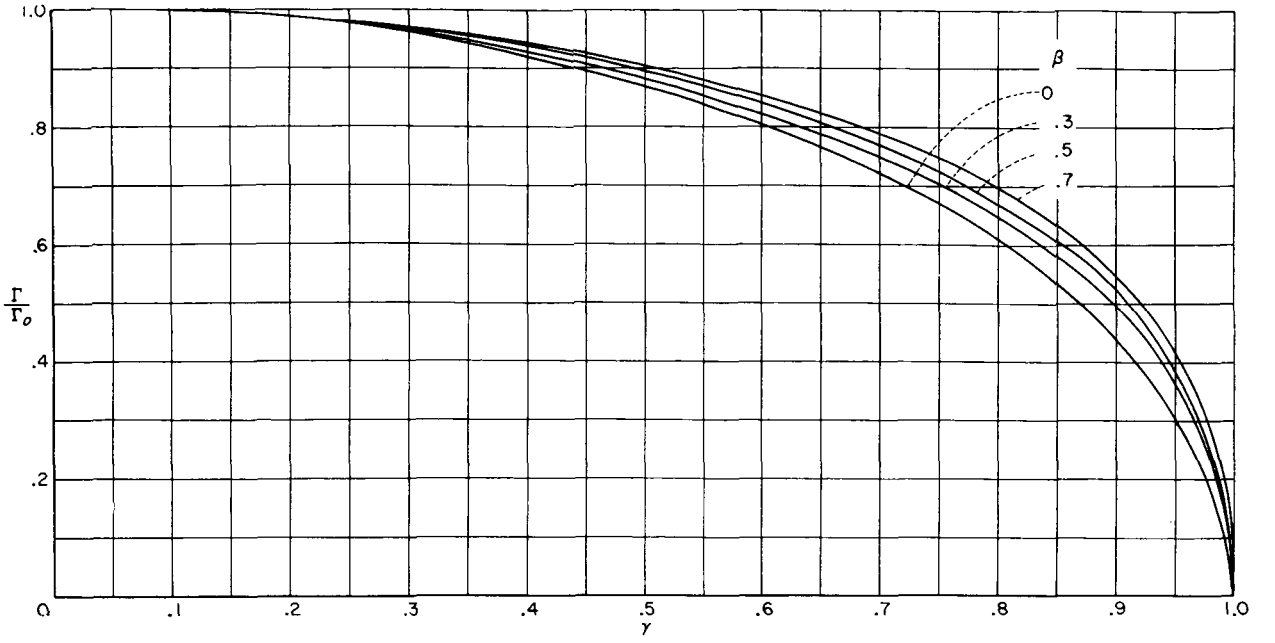

FIGURE 28.—The optimum nondimensional circulation distribution for several semiellipse arcs.

In connection with the forms discussed previously, it should be noted that the direction in which the arc or arc system lifts is immaterial; the value of k depends only upon the curvature of the arc. Thus the two identical arcs shown in figure 29 have the same induced drags for the same lift force. In practice, however, one orientation may prove more convenient than another for a specific application. The induced lift for the two orientations is not the same. The induced lift is positive when the local aerodynamic force acts towards the local center of curvature of the arc and negative when this force is directed outward from the center of curvature.

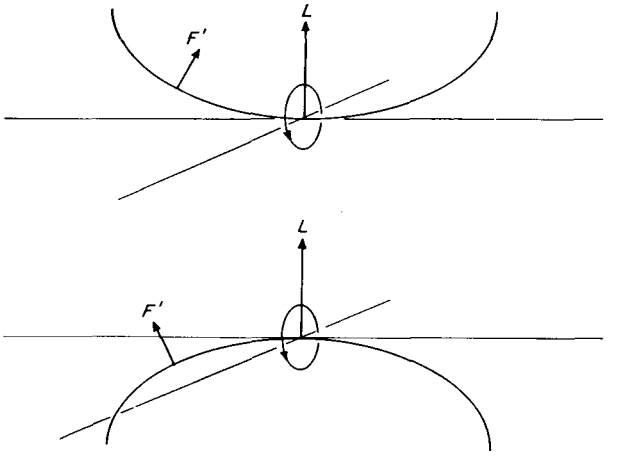

FIGURE 29.—Identical lifting arcs with different orientations of the lifting force.

SOLUTIONS FOR MORE COMPLEX SYSTEMS

Although single arcs of moderate curvature offer an attractive means for increasing aerodynamic efficiency because of their simple structural forms, it is desirable to consider more involved geometrical arrangements so as to gain an idea of the relative values of effective aspect ratio obtainable with more complex systems. The purpose of this section, therefore, is to determine the efficiency factor for a number of such lifting systems and to draw some general conclusions as to the effects of geometry variation on aerodynamic efficiency. In general, the forms to be investigated are such that they may be considered as derived from the basic flat span by various modifications to the outer or tip sections, while the flat center portion of the span is left unchanged. A few complex systems will be considered in which the total span is altered. The term "complex" as used here is intended to describe a lifting system made up of a series of superposed arcs or segments, as opposed to a "simple" system consisting of a single arc or line. All the results of this section were obtained by use of the electrical analog.

TIP MODIFICATIONS

End plates and vertical fins.—End plates and vertical fins located near the tips of the wing have long been used to increase aerodynamic efficiency at high lift coefficients. Three commonly used configurations have been investigated by use of the analog, and the results are shown in figure 30. Comparison of the values of k for forms A and B clearly shows the beneficial effect, from an induced-drag standpoint, of using large end plates. Comparison of forms A and C, representing an end plate or tip fin and an inboard fin, respectively, shows the detrimental effect of moving the fin inboard (a decrease in k from 1.22 to 1.14). In such a case, much of the trailing vorticity is shed inside of the tip and, as may have been anticipated, leads to increased induced drag compared with that at the tip location. Still, the inboard fins provide an increase in L/D_i over that of the flat elliptical wing. In considering increases in effective aspect ratio, it must be realized, of course, that only increases in the factor L/D_i are revealed. Since profile and parasite drag always accompany the physical wing system, the actual gains in L/D must always be less than those in L/D_i. This effect will be considered in more detail in the next section.

In the use of end plates or fins to increase the effective aspect ratio of wings, care must be taken to see that the end plate or fin is designed to operate with the optimum circulation distribution if the large values of k indicated in figure 30 are to be realized. In the past, actual plates (no camber) or plain symmetrical sections have often been used to construct end plates which merely served as simple physical barriers against the spanwise flow. In order to realize the full aerodynamic advantages of such devices, however, care must be given to more exact design of the fins for optimum operational loadings. Much of the original experimental data taken to evaluate the aerodynamic efficiency of wings with end plates are based on the use of such "shields" and are thus not truly indicative of the results possible with more carefully designed fins.

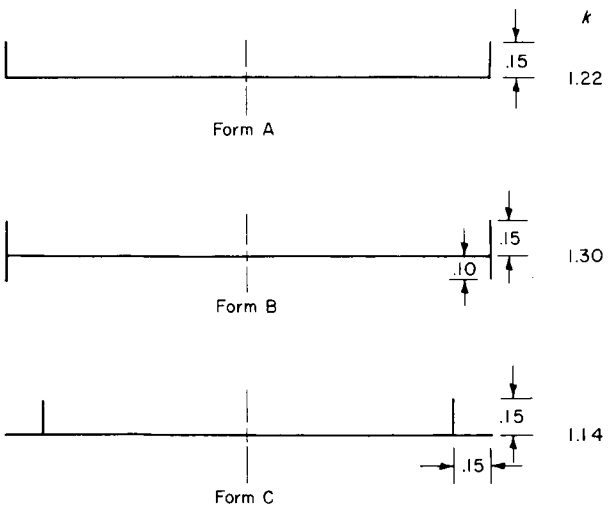

FIGURE 30.—Efficiency factors and geometry of end-plate forms. All dimensions are given in fractions of the semispan length.

Treatment of many end-plate and fin configurations by conformal mapping techniques is extremely difficult, even for very simple forms (ref. 7). Thus the analog method provides an especially simple and valuable means for analysis of such systems. Since many approximations usually must be made in treating such problems by conformal analysis, the final accuracy of such results cannot generally be expected to exceed that of the analog procedure.

Curved tips.—A series of forms obtained by curving only the outer part of the span is shown in figure 31. In form A the outboard quarter of the semispan consists of a circular arc, as shown. The reason for using such a shape is to move the tip region of the wing, where the strongest vorticity is shed (large $d\Gamma/ds$), away from the heavily loaded center of the span and thus reduce the downwash at the center. The value of $k=1.23$ for this form is quite high. By adding a second arc as in form B the increment in k is about double that of the single arc. In closing the tip region between the arcs (form C), the very high value of $k=1.52$ is obtained. Form D has the tip curved into a semiellipse of eccentricity $e=0.82$.

Closed-arc tips.—An interesting series of tip modifications is that obtained by adding various symmetrical closed curves at the wing tip, as shown in figure 32. Forms A and B show the effects of ending the span in circles of various sizes. These curves appear to be highly efficient in increasing the effective aspect ratio, even for the small circle. Forms C, D, E, and F show tips formed of closed ellipses with various orientations. It is clear that the ellipses alined with the

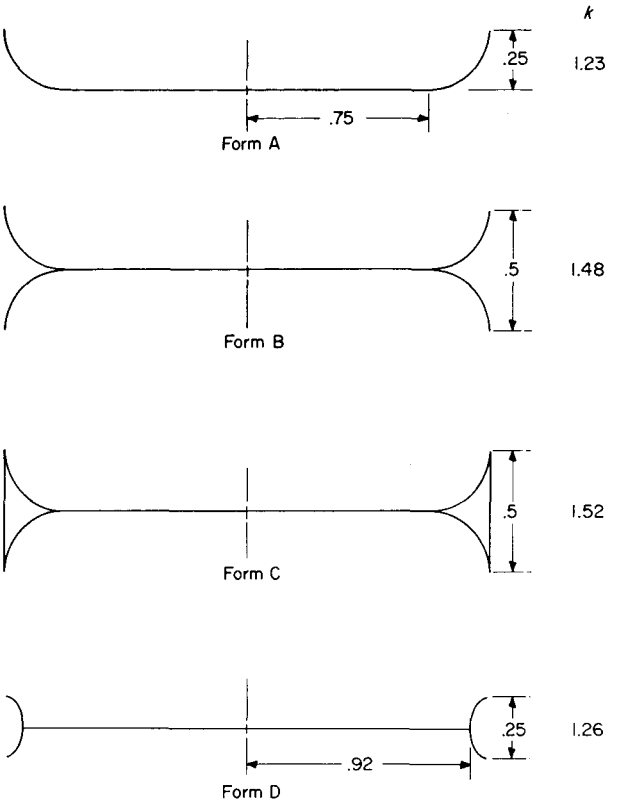

FIGURE 31.—Efficiency factors and geometry of curved-tip forms. All dimensions are given in fractions of the semispan length.

major axis vertical are considerably more efficient in increasing the effective aspect ratio than are the ellipses with major axis alined with the horizontal, in accord with the principle of vorticity spreading. It also appears that a vertical ellipse with large eccentricity is more efficient than one with smaller eccentricity.

It should be emphasized perhaps that the closed tips just discussed are not solid areas or bodies at the tip, but are formed by open areas bounded by a lifting line or arc. The free-stream air passes through the open area of these tips. In fact, the wake of these forms consists of the core of irrotational air which has passed through the tips, surrounded by the closed vortex sheet emanating from the boundary. This enclosed core of air has no circulatory motion within it (as opposed to the normal tip vortex) and translates downward with the speed w_o normal to itself far downstream.

Branched tips.—Another form of tip modification consists of splitting the tip section of the

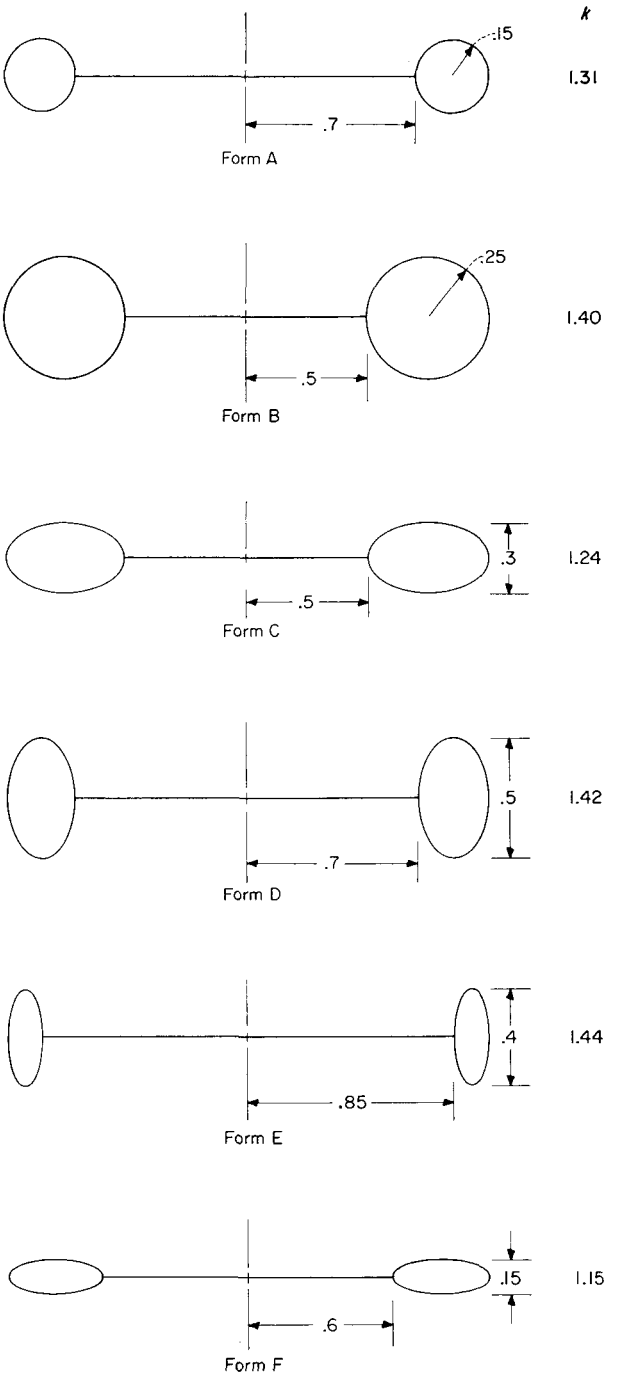

FIGURE 32.—Efficiency factors and geometry of closed-arc tip forms. All dimensions are given in fractions of the semispan length.

span into several separate branches or arcs, and may be considered as an extension of the curved-tip forms. Several such branched-tip forms are shown in figure 33. Forms A, B, and

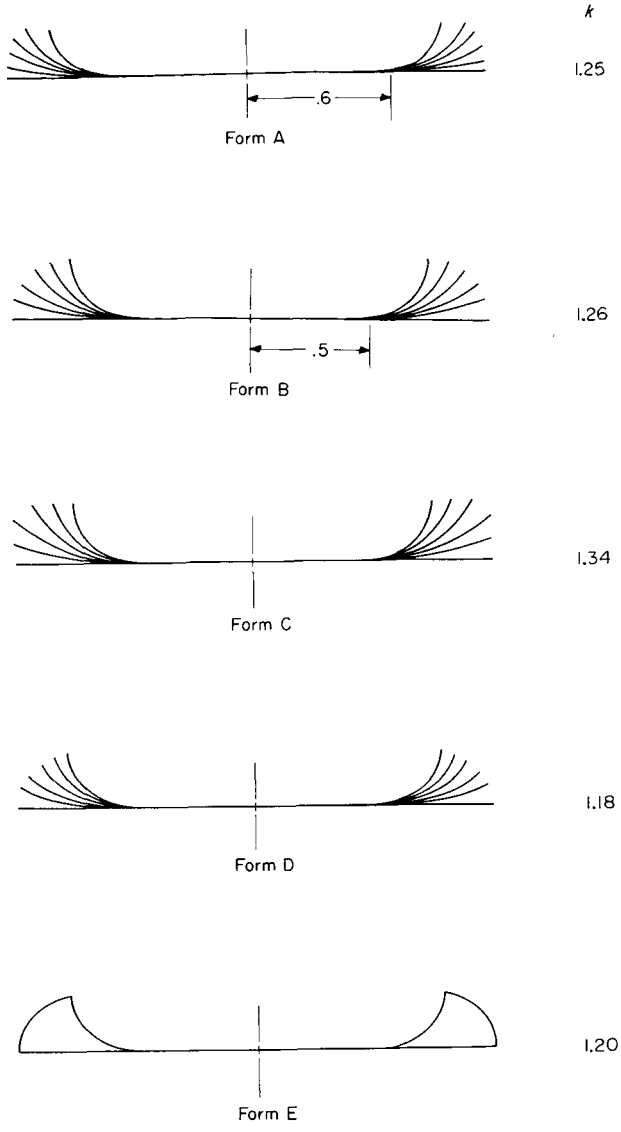

FIGURE 33.—Efficiency factors and geometry of branched-tip forms. All dimensions are given in fractions of the semispan length.

C are derived by using circular-arc segments and are constructed according to a definite pattern. Form A is composed of circular-arc segments in which the arc length of each branch is equal to a specified percentage of the semispan and the various branches are identified by their camber β (where β has the same definition as previously given for circular arcs). For form A, the arc length of the first branch is equal to $\frac{1}{3}$ the semispan, while all other arcs are $\frac{5}{12}$ of the semispan. Forms B and C are constructed according to a similar rule. Such forms give relatively large increases in effective aspect ratio, are relatively simple in geometry, and offer the possibility of aeroelastic construction, as is discussed subsequently. Forms D and E are composed of elliptical branches, and are less efficient than the circular forms, for the relative sizes used. Form E is the same as form D except that an outer boundary has been added to close the gaps at the outer extremities of the branches. Only a slight increase in efficiency is gained by closing the gaps. This result follows from the fact that the vertical flow is already nearly equal to w_o everywhere in the region between the branches even before the closing boundary is added.

Some ambiguity may exist as to the manner in which the analog potential readings are to be made on such branched-tip forms. To clarify this point, figure 34 is presented, which shows the integration path used to determine the circulation corresponding to a given spanwise station y, for an arbitrary branched-tip form. The electrodes may be placed on points 1 and 4 to obtain the circulation around arc segment B and then on points 2 and 3 for arc segment A; the total value of ΔE is the sum of all such readings. Alternately, readings can be made at points 1 and 2 and points

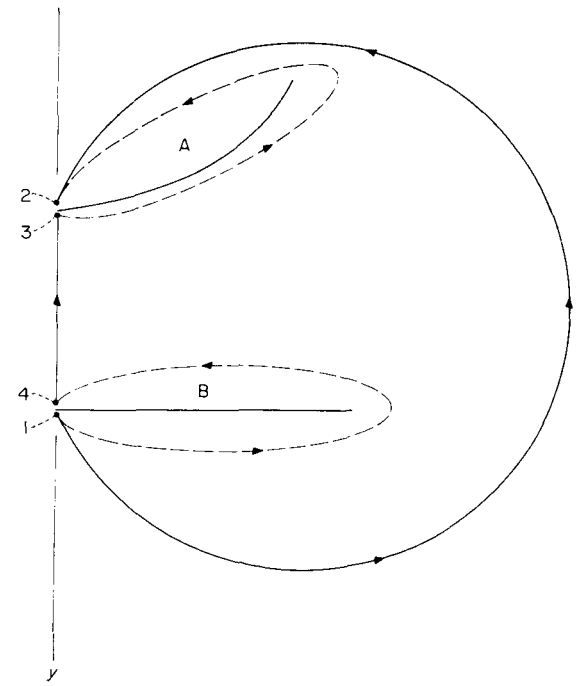

FIGURE 34.—The paths of integration for branched-tip forms.

3 and 4 separately and the results added algebraically. This procedure can be followed because of the condition that $\Delta E_{1,2}=\Delta E_{1,4}+\Delta E_{4,3}+\Delta E_{3,2}$ since the change in potential must be zero when passing around any closed circuit which does not include a part of the boundary slit. The subscripts represent the end points of the path as shown. In the case of most of the branches of the forms of figure 33, the internal paths (such as between points 4 and 3 in fig. 34) have $\Delta E=0$, and this condition indicates that the velocity between the branches is zero. This result may be regarded as an experimental proof of Munk's results, which predict that the sum of the vertical velocity of the free-stream wake flow $-w_o$ and the induced velocity inside a closed lifting curve will be zero when the lifting curve is optimally loaded (ref. 2).

TOTAL-SPAN MODIFICATIONS

Closed semicircle.—Figure 35(a) shows a closed semicircle wing. The k value for this form is 1.50, the same as was previously found for an open semicircular arc. In fact, it can be shown that the flow regimes for the two forms are practically identical. This fact indicates that for minimum induced drag with the closed form, the flat side must remain essentially unloaded.

Semicircle with extensions.—The semicircle form with flat span extensions shown in figure 35(b) shows very little gain in effective aspect ratio ($k=1.07$), despite the relatively large change in geometry as compared with the flat-span wing. When large end plates are added to this form, such as shown in figure 35(c), the value of k is raised to 1.30. As might be expected, closing the open side of this form with end plates was found to have no effect on k.

GENERAL CONCLUSIONS

The brief considerations of this section indicate that appreciable gains in the effective aspect ratio can be obtained by relatively minor alterations to the tip region of flat wings for equal spans. Some tip alterations can result in far greater efficiency increases than those produced by radical modification of the entire span. For the forms investigated here, it appears that modifications which tend to release the major portion of the vorticity near the tip and over an appreciable vertical area result in the greatest increases in k. For the forms considered, it appears that increases in k of 30 to 50 percent are possible. On such forms as the branched-tip series, considerable increases in k are possible by extending the arc lengths of the branches while the span is maintained constant.

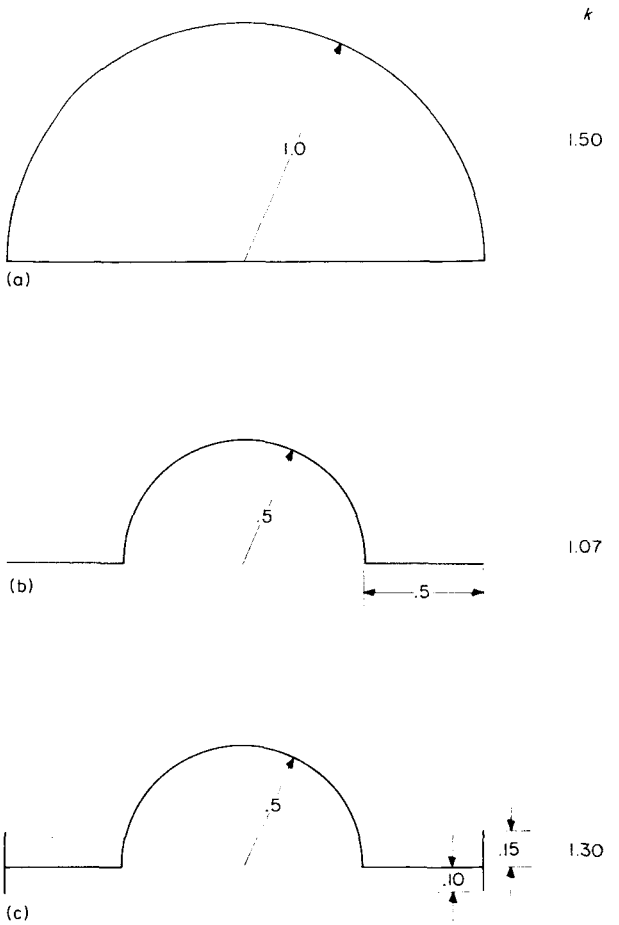

(a) Closed semicircle wing.

(b) Semicircle wing with flat span extensions.

(c) Semicircle wing with flat span extensions and end plates.

FIGURE 35.—Efficiency factor and geometry of closed and modified semicircle forms. All dimensions are given in fractions of the semispan length.

The results of this section serve to illustrate the variety of complex forms which can be treated with the analog. These procedures can be used not only to establish the efficiency of arbitrary forms but also to determine the effective aspect ratio for wings with the span shape $z(y)$ set by other design considerations.

THE INDUCED LIFT OF NONPLANAR SYSTEMS

Unlike flat-span wings, nonplanar wings have a component of induced velocity in the streamwise

direction due to the bound vorticity and, depending upon the lifting orientation of the system, this velocity can be beneficial in increasing the lift of the system for a given induced drag. While for most systems the magnitude of the induced lift is probably small, it is possible that some highly curved arcs, say a semicircle, may have a measurable induced lift.

THE INDUCED-LIFT INTEGRAL

With the use of the simple arc form and definitions of figure 36, it can be shown that the induced lift L_i is given by the relation

$$L_i=\frac{\rho}{4\pi}\int_{-s_t}^{s_t}\Gamma(s)\left[\int_{-s_t}^{s_t}\Gamma(s')\frac{\sin\omega}{r^2}ds'\right]\cos\tau ds \quad (99)$$

Thus, when the value of the optimum function $\Gamma(s)$ has been determined by means of the foregoing procedures for a given arc form $z=z(y)$, the induced lift accompanying this distribution of circulation can be determined by equation (99). The induced-drag efficiency parameter then becomes

$$\frac{L+L_i}{D_i} \quad (100)$$

EFFECT OF LIFT ORIENTATION

If the lifting arc is oriented such that the aerodynamic force intensity F' is in the direction of the local center of curvature (fig. 29) the sign of L_i will be positive and a gain in efficiency will result. If the force acts away from the center of curvature, the sign of L_i will be negative and a decrease in efficiency will result. These effects of bound-vorticity induction might be classified as a type of "interference" effect. A practical example of this interference is in the location of end plates on a wing (fig. 37). If the end plate is mounted entirely above the wing (fig. 37(a)), a favorable interference should result (L_i positive). If mounted below (fig. 37(b)), the interference should be unfavorable (L_i negative). When mounted symmetrically (fig. 37(c)) there should be no net value for L_i.

In estimating efficiencies of highly curved simple systems and of complex systems, the effects of the induced lift should be considered. The magnitude of the effect, of course, will depend upon the geometry and lift intensity of the particular system.

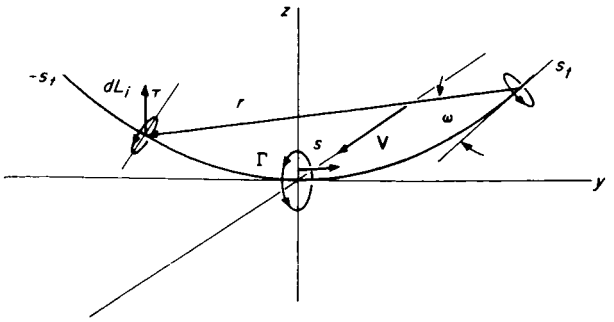

FIGURE 36.—Geometry and velocity relations for determining the induced lift of nonplanar systems.

PRACTICAL APPLICATION CONSIDERATIONS

As has already been pointed out, successful practical application of nonplanar wing forms for improving aerodynamic efficiency depends entirely upon the ability to construct such wings with a sufficiently low structural weight and profile drag. The nature of the structural-aerodynamic interrelations can be seen from the following considerations. If it is assumed that an

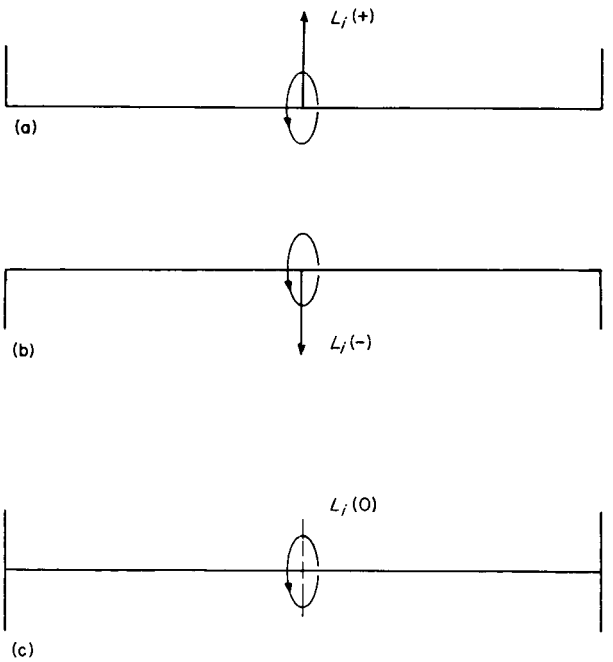

(a) End plates mounted entirely above wing.

(b) End plates mounted entirely below wing.

(c) End plates mounted symmetrically.

FIGURE 37.—Interference (induced lift) effects occurring with end plates.

"optimum" flat wing of span b and area S has already been chosen for a particular set of mission requirements, it is desirable to examine various nonplanar forms to see whether the basic wing efficiency can be improved. For illustration purposes, the nonplanar form is taken in the following discussion as the semiellipse shown in figure 38. If the wing area S of the given flat wing is used as the basis for defining the force coefficients of the cambered wing, the induced-drag polar of the nonplanar form is given by equation (48)

$$C_{Di}=\frac{C_L^2}{\frac{K}{\psi^2}A}$$

where K is an absolute constant which depends only upon the camber factor β of the arc (for the optimum circulation loading) and ψ is the span comparison ratio which gives the length of the projected span b' of the curved wing in terms of the span b of the flat wing, $b'=b/\psi$ (eq. (46)). The factor ψ clearly indicates the actual physical size of the curved wing in relation to that of the flat wing. Thus, the induced-drag efficiency of the curved wing, $k=K/\pi\psi^2$, is a function of its physical span length b' (fig. 38).

However, the structural weight and profile drag of the curved wing are also functions of its physical size. If the case where $b'=b$ is considered (i.e., $\psi=1.0$), it is evident that the physical arc

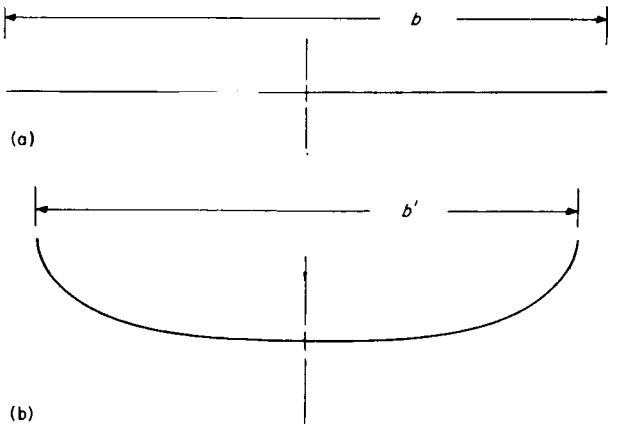

(a) Flat span elliptical planform.

(b) Elliptically cambered span.

FIGURE 38.—Comparison of a flat elliptical-planform span with an elliptically cambered span.

span length s_T of the curved wing, where

$$s_T=\int_{-s_t}^{s_t} ds=\int_{-b'/2}^{b'/2}\sqrt{1+\left(\frac{dz}{dy}\right)^2}dy \qquad (101)$$

is always greater than that of the flat wing span b, or

$$s_T>b'=b \qquad (\psi=1.0) \qquad (102)$$

This increase in physical length must be considered in terms of the structural weight of the wing as compared with the weight of the flat wing. In addition, the greater arc length must be considered in terms of the total surface area of the structure exposed to skin friction and pressure drags. Neither of these factors can be allowed to be significantly greater than those of the flat wing since any increase at all proportionately detracts from the gains due to the higher effective aspect ratio. If b' is decreased (i.e., ψ made greater than 1.0), the physical size of the curved wing decreases; thus both the structural weight and profile drag are reduced. Simultaneously, however, the induced drag of the wing increases, since the effective aspect ratio of the wing decreases. (See eq. (48).) Thus, by expressing the wing structural weight and profile-drag coefficient as functions of ψ, the optimum span of the curved wing corresponding to minimum total drag for a specified lift force can be determined. This minimum drag can then be compared with that of the flat wing at design lift and the relative efficiencies of the two forms evaluated.

The successful working out of these problems depends entirely upon the availability of efficient structural techniques, and since the nature of the design compromises necessary will depend entirely upon the mission requirements of the particular aircraft under consideration, no general statements can be made on the net gains in efficiency possible with cambered-span airfoils. There are, however, two immediate approaches to the weight and profile-drag problems which may be of fairly general applicability.

The first approach involves aeroelastic wing construction in which the desired spanwise camber $z(y)$ of the wing is obtained by the "designed" elastic deformation of the span under the optimum airload of the cruise flight conditions. That is, a considerable reduction in wing weight might be attained by making the wing sufficiently elastic that the span will assume the desired

curvature under the loading condition of cruise flight. Since the bending-moment distribution along the span of a wing (together with the shear) determines the necessary section moment-of-inertia distribution $I(y)$, it follows from the bending-moment relation for large curvatures

$$M(y)=EI\frac{\frac{d^2z}{dy^2}}{\left[1+\left(\frac{dz}{dy}\right)^2\right]^{3/2}} \tag{103}$$

that the wing moment-of-inertia distribution $I(y)$ (and hence the weight per unit of span) can be made very small if the curvature under design loading

$$\frac{d^2z}{dy^2}\left[1+\left(\frac{dz}{dy}\right)^2\right]^{-3/2} \tag{104}$$

is sufficiently large. Thus, for certain camber functions $z(y)$, the weight of an elastic-span wing possibly can be made equal to or less than that of the equivalent flat-span wing (where the curvature parameter is very small under flight air loads). In addition, certain cambered wing forms offer the possibility of simple bracing methods which can result in very light structural weights.

The second approach involves the use of laminar-flow airfoil sections to reduce the total skin-friction drag. Certain laminar-flow profiles (such as the NACA 64_3-618 airfoil) have an extensive low-drag lift-coefficient range and a very high thickness ratio. Since the drag coefficient is practically independent of lift coefficient for such profiles, even up to very high C_L values (C_L=1.1), use of these sections operating at a relatively high section lift coefficient can reduce the local chord length and thus produce the required lift with a decrease in total profile drag and structural weight. The chord size reduction is limited by the maximum wing lift coefficient desired. This method appears highly suitable, however, for those sections of highly curved spans which produce primarily side force. The thickness of these profiles is especially valuable in providing sufficient depth for housing wing spars. In the application of such profiles to cambered-span wings, due consideration, of course, must be given to the effect of span curvature on the stability of the laminar boundary-layer flow.

In general, nonplanar wings will be designed to possess the optimum span loading for the cruise flight condition, and at other angles of attack the efficiency must decrease if the wing structure is rigid or fixed, because of the changes which occur in local angle of attack with nonplanar wings as the whole wing is pitched. With variable geometry or elastic spans, however, it may be possible to maintain optimum loadings over a considerable lift-coefficient range. The design of nonplanar wings for optimum span loading at given cruise conditions is relatively simple, since the effective downwash at each point of the span can be directly determined by use of the foregoing theory.

Aside from efficiency gains, there are other possible advantages offered by nonplanar wings for specific applications. For example, the vertical arrangement of the lifting elements offers the possibility of obtaining longitudinal stability and control without the need for a tail plane. Such systems also offer a wider latitude in lateral and directional control than do flat wings. When conventional tail-plane control is used, the spreading of the vortex wake by use of nonplanar wings, combined with the lower wake downwash velocities of these systems, can offer possible solutions to high-lift stability and control problems.

The foregoing procedures can also be used to investigate a number of other important problems in aircraft design. When large amounts of geometrical dihedral, or anhedral, are required in wings for proper lateral static and dynamic stability characteristics, the wing span loading necessary for minimum induced drag can be determined with dihedral effects included. The proper span loading of special wing forms such as gull and inverted-gull wings can be determined in a simple manner. Finally, since the entire flow field of the vortex wake is given by either the conformal or analog method, the "downwash" field necessary for longitudinal stability analyses on such wings can be calculated.

CONCLUDING REMARKS

The intention of this investigation has been to outline the basic theoretical concepts and procedures necessary for determining the induced lift and the minimum induced drag for arbitrary nonplanar lifting systems. The results have shown that it is possible to describe the induced-drag efficiency of such systems in terms of an

effective aspect ratio, and that this aspect ratio can be simply determined even for complex systems by use of the electrical potential-flow analog. The theory also provides the downwash field information necessary for designing physical wing systems which will possess minimum induced drag for a given lift force.

Application of the theoretical results to the prediction of the effective aspect ratio of a number of simple and complex lifting systems of equal spans has indicated that significant reductions in induced drag can be obtained by use of nonplanar lifting forms. It appears that cambered-span wings can increase the effective aspect ratio as much as 50 percent compared with the flat, elliptical-planform wing having equal span and producing equal lift, but the overall efficiency increase depends also upon the structural weight and profile drag of the cambered forms.

A brief analysis of the problems and requirements which must be satisfied for successful practical application of nonplanar wings has indicated that in many cases structural considerations will most probably govern the magnitude of the efficiency improvement which can be actually realized.

Various methods for overcoming the weight and profile-drag problems which may be expected with some of the forms investigated appear feasible in the light of advances in aeroelasticity technology and in low-drag wing profile developments. Wings with a designed aeroelastic deformation program can probably result in the realization of a significant part of the theoretically possible gains in aerodynamic efficiency.

LANGLEY RESEARCH CENTER,
NATIONAL AERONAUTICS AND SPACE ADMINISTRATION,
LANGLEY STATION, HAMPTON, VA., *February 21, 1962.*

REFERENCES

1. Cone, Clarence D., Jr.: A Theoretical Investigation of Vortex-Sheet Deformation Behind a Highly Loaded Wing and Its Effect on Lift. NASA TN D-657, 1961.
2. Munk, Max M.: The Minimum Induced Drag of Aerofoils. NACA Rep. 121, 1921.
3. Von Kármán, Th., and Burgers, J. M.: General Aerodynamic Theory—Perfect Fluids. Vol. II of Aerodynamic Theory, div. E, ch. III, sec. 16–22, W. F. Durand, ed., Julius Springer (Berlin), 1935 (reprinted by Durand Reprinting Committee, 1943), pp. 125–139.
4. Milne-Thomson, L. M.: Theoretical Aerodynamics. Second ed., Macmillan and Co., Ltd., 1952.
5. Weissinger, Johannes: Zur Aerodynamik des Ringflügels in inkompressibler Strömung. Z. Flugwissenschaften, Jahrg. 4, Heft 3/4, Mar./Apr. 1956, pp. 141–150.
6. Fletcher, Herman S.: Experimental Investigation of Lift, Drag, and Pitching Moment of Five Annular Airfoils. NACA TN 4117, 1957.
7. Mangler, W.: The Lift Distribution of Wings With End Plates. NACA TM 856, 1938.

U.S. GOVERNMENT PRINTING OFFICE: 1963